

FINAL TECHNICAL REPORT

USGS NEHRP AWARD #06HQGR0040

**LINEAR AND NON-LINEAR WAVE PROPAGATION STUDIES WITHIN
SEDIMENTS OF THE MISSISSIPPI EMBAYMENT**

Charles A. Langston

Zack Lawrence

Center for Earthquake Research and Information

University of Memphis

3876 Central Ave., Suite 1

Memphis, TN 38152-3050

Telephone: (901)-678-4869

Fax: (901) 678-4734

Email: clangstn@memphis.edu

April 22, 2008

ABSTRACT

USGS NEHRP AWARD #06HQGR0040, *LINEAR AND NON-LINEAR WAVE PROPAGATION STUDIES WITHIN SEDIMENTS OF THE MISSISSIPPI EMBAYMENT* by Charles A. Langston and Zack Lawrence, Center for Earthquake Research and Information, University of Memphis, 3876 Central Ave., Suite 1, Memphis, TN 38152-3050. Telephone: (901) 678-4869, Fax:(901) 678-4734, Email:clangstn@memphis.edu

A series of seismological experiments were performed in Arkansas and Tennessee to investigate linear and non-linear wave propagation effects within the unconsolidated sediments of the Mississippi embayment. The scientific purposes of these experiments were to develop models of the sediments that faithfully reproduce the waveforms of explosion strong ground motions, collect specific data to experimentally verify the basic wave physics of empirical seismic techniques in site characterization, and to investigate *in situ* methods of determining soil non-linearity that impact strong ground motion estimates in major seismic zones. Seismic reflection and refraction data using P and SH wave sources were collected near the explosion sites of the 2002 Embayment Seismic Excitation Experiment(ESEE) to derive constraints on sediment velocity structure that could be incorporated into waveform modeling of near-source strong motion array data. The reflection data set collected at Mooring, TN, led to the exciting discovery of an intense micro-earthquake swarm that may be the manifestation of non-volcanic tremor associated with the Reelfoot fault. This serendipitous discovery alone justifies our data collection efforts and suggests that there are intriguing and important new fault zone processes to investigate in the New Madrid seismic zone that have significant impact on knowledge of seismic hazards.

We investigated the physical basis of Nakamura's H/V method for determining site resonance and amplification characteristics of thick sediments by deploying a phased,

broadband array near the Marked Tree site of the 2002 experiment. Background noise data were collected and analyzed to determine the wave parameters of the microseismic noise field. Additionally, we analyzed data from a smaller array experiment deployed near the northern explosion site of the 2002 experiment using new wave gradiometry techniques to also determine wave parameters. We discovered that the microseismic noise wavefield is relatively coherent near the H/V resonant peak for these sites and correlates in azimuth with high wave height regions in the North Atlantic. Analysis of the array data and broad band data taken from a station outside of the embayment shows that sediments of the embayment amplify ambient noise by an order of magnitude but that amplification is due to the conversion of high phase velocity Rayleigh waves into shear body waves that become trapped in the unconsolidated sediments. The position of the spectral peak is consistent with body wave resonance models but the amplitude depends on a particular wave propagation mechanism that might not be important for local S wave propagation from large earthquakes

An array of strong motion accelerographs and a NEES consortium shaker truck were used to detect and investigate soil non-linearity at a site near Blytheville, AR. Strong harmonic ground motions were produced by the vibroseis source and recorded by an immediately adjacent array of seismographs. Soil non-linearity was evident from changes in frequency-dependent Rayleigh wave phase velocities as a function of input force level in the vibroseis source. In addition, particle motion analysis indicates the effect of changing attenuation through tilting of Rayleigh wave particle motion ellipses. This kind of experiment is a practical way of obtaining non-invasive data on soil non-

linearity that may be used in the analysis of hazards from earthquake strong ground motions.

INVESTIGATIONS UNDERTAKEN

We investigated the elastic and anelastic properties of unconsolidated sediments of the Mississippi embayment using standard seismic field methods, earthquake data from the Center for Earthquake Research and Information (CERI) seismic network, previously collected strong motion data from the 2002 Embayment Seismic Excitation Experiment, reflection data from the 1981 Mississippi River reflection experiment, and a new strong motion experiment using a strong Vibroseis source. The goal of this research is to produce detailed 1D velocity models for 3 sites in the embayment that predict the frequency content and waveforms of local earthquakes and explosions. We want to place very tight bounds on velocity structure, attenuation structure, and the nature of low and high strain wave propagation at these sites to understand how the unconsolidated embayment sediments will respond to strong ground motions from future large earthquakes in the region.

A synopsis of the work of this grant is given in Table 1.

<p><i>Field Work</i></p> <p><i>Collect small-scale refraction/reflection/surface wave data:</i> <i>Marked Tree Explosion and K2 Array Site</i> <i>Mooring Explosion and K2 Array Site</i> <i>Blytheville Site</i></p> <p><i>Collect earthquake data from CERI station at Mooring</i> <i>Install and operate a broadband array to collect H/V data</i> <i>Marked Tree K2 Array Site</i> <i>Mooring K2 Array Site</i></p> <p><i>Non-linear Wave Propagation Experiments</i> <i>Blytheville Site</i></p>
<p><i>Field Data Reduction</i></p> <p><i>Produce layered earth structure models for each site using travel-time analysis, reflection imaging, and high frequency surface wave dispersion inversion</i> <i>Examine site resonance in earthquake data recorded at Mooring</i> <i>Array analysis of array data to understand the ambient seismic noise field and relate it to H/V measurements and local earth structure</i> <i>Determine modulus reduction of near-surface materials using frequency/wavenumber</i></p>

<i>array analysis from data of the explosion experiments</i>
<i>Waveform modeling</i>
<i>Produce layered earth models for the ESEE K2 array data using the results from the field studies. Use to predict observed strong ground motions. Joint inversion of the field data and strong motion data if needed.</i>
<i>Evaluate the effect of non-linear modulus reduction determined from the Vibroseis experiment on strong ground motions by developing equivalent linear models.</i>

Table 1: Experiments and scientific activities for this project

Although much of this work was performed as originally proposed, field conditions and new experimental methodologies offered new ways to collect data and to obtain more highly controlled experiments. In particular, because the 2002 explosion sites and K2 array sites were so close together (within ~2km for both explosions) it was deemed acceptable to simply run 0.5-0.7km reflection and refraction lines along unpaved farm roads between the explosion and array points rather than collecting data at each point. We also replaced the previously proposed explosion experiment for investigating soil non-linearity with an experiment that involved creating strong ground motions from a Vibroseis truck. This was done because of a pilot experiment that was run by one of the P.I.s (P.B.) previous to this research.

But, perhaps, the most exciting results from this research were found completely by accident. While performing the reflection/refraction experiment at the Mooring site, we recorded a remarkable series of microearthquakes in November 2006 that may be an indication of non-volcanic tremor occurring on or near the Reelfoot fault. Analysis of the raw reflection shot gathers indicate a seismicity rate of 257 to 1029 M_L -1 to -2 earthquakes per hour which is 2 to 3 orders of magnitude higher than the background seismicity rate using the

Gutenberg-Richter relation (see below). Such a high seismicity rate is reminiscent of continuous non-volcanic tremor observed in the Cascadia subduction zone [Dragert *et al.*, 2001] associated with episodic plate slip or at deeper levels of the San Andreas fault [Nadeau and Dolenc, 2005]. The occurrence of non-volcanic tremor in the New Madrid fault zone represents a significant discovery that should give clues on the stress and rheological state of the crust in North America's most dangerous intraplate fault zone. We believe this observation and more recent observations of earthquake swarms within the NMSZ warrant a focused observational campaign to detect, locate, and characterize non-volcanic tremor in the NMSZ.

Scientific Leverage

Table 1 shows that work on this grant consists of at least 3 major, field-intensive experiments with related, yet separate, immediate scientific goals. The additional discovery of possible non-volcanic tremor in the NMSZ is a 4th study that was not anticipated. The collection of each data set is a valuable contribution to the community that can be used in further research and in the classroom. Indeed, we are still modeling and analyzing the seismic data in our research and expect that the data will form the basis of many future scientific publications and student thesis projects long after this final technical report has been submitted. In addition, many of the seismic instruments, particularly the broadband seismometers and K2 accelerographs used in the seismic array experiments, came from the CERI instrument pool.

Personnel

Co-Principal Investigator Paul Bodin left CERI in early August 2006 for a new position at the University of Washington. Dr. Bodin was the investigator primarily responsible for field deployments and was unavailable for continuing project fieldwork. However, he has been in continual contact with Zack Lawrence, whom he co-advised, on work pertaining to the Blytheville experiment on non-linear soil effects and has contributed to the scientific analysis of data sets.

Because this project has been fieldwork-intensive, there have been many graduate students and additional research scientists at the earthquake center (CERI) who have helped prepare instrumentation or who have accompanied the P.I. into the field for various deployments (Table 2). In addition, Robert Williams and David Worley from the Denver office of the U.S. Geological Survey volunteered seismic equipment and a day of their time so we could collect Vibroseis P wave reflection/refraction data and SH reflection/refraction data at the Mooring site.

<i>Mooring Broadband Array Noise Experiment (2002)</i>	
Charles Langston Paul Bodin Stephen Horton John Filipcic Buck Grant	P.I. Co P.I. Research Scientist Technical Staff Graduate Student (data analysis)
<i>Marked Tree Broadband Array Noise Experiment</i>	
Charles Langston Zack Lawrence Buck Grant	P.I. Graduate Student Graduate Student
<i>CERI Network Data</i>	
Christy Chiu	Staff Scientist
<i>Mooring Reflection/Refraction Experiment</i>	
Charles Langston	P.I.

Rob Williams Dave Worley Christopher Stanton Ting-Li Lin Zack Lawrence Duayne Rieger	U.S.G.S. U.S.G.S. Graduate Student, UT Austin Graduate Student Graduate Student Undergraduate Student (data analysis)
<i>Marked Tree Reflection/Refraction Experiment</i>	
Charles Langston Ivan Rabak Ting-Li Lin Buck Grant	P.I. Graduate Student Graduate Student Graduate Student
<i>Blytheville Non-Linear Experiment</i>	
Paul Bodin Zack Lawrence Charles Langston Stephen Horton	Co-P.I. Graduate Student P.I. Research Scientist

Table 2 – Personnel associated with fieldwork or data analysis related to this grant.

FIELD EXPERIMENTS AND DATA

Mooring Site

Figure 1 is an index map showing the location of the Mooring site where a 5000 lb blast was detonated in October 2002 as part of the ESEE [Langston *et al.*, 2006]. The K2 array data are extensively discussed in that publication. One of the ultimate goals of this work is to be able to model the waveforms of the strong ground motions to high fidelity to obtain the velocity and attenuation model between source and receiver. Although it is possible to model the waveforms using travel time and amplitude information of the strong motion data themselves, constraints on the velocity structure are needed to understand the major wave propagation mechanisms seen in the strong motion data. On November 16, 2006, in conjunction with the U.S. Geological Survey, we

collected P and SH reflection/refraction data along a 0.7km profile midway between the shot point and K2 array to provide average velocity constraints.

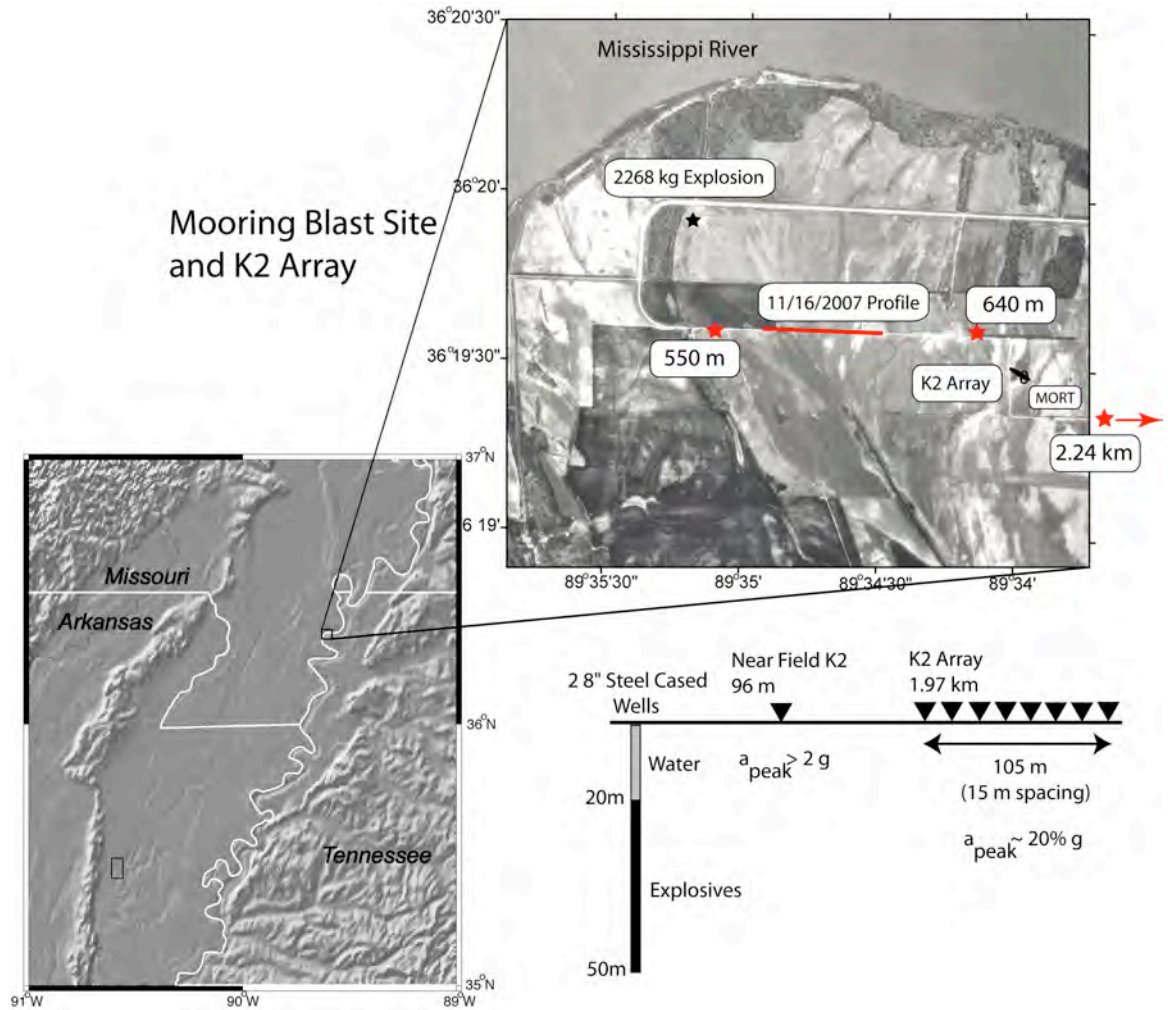


Figure 1 – Index map for the Mooring, TN, site of the 5000 lb ESEE shot. Locations of the ESEE shotpoint, the 8-element K2 array that recorded strong ground motions from the shot, the CERI network station MORT, and the 16 November 2006 reflection/refraction profile with related far-offset shot points are all shown in the panel to the upper right. The geometries of the ESEE shot point and K2 array are shown in the lower right. The location of the 2002 broadband noise experiment array is about 1 km east of MORT station.

As part of another reflection profiling project, the U.S.G.S. was in the area with reflection gear and also had use of the UT Austin “Thumper” vibroseis truck from the

NEES consortium. Rob Williams graciously offered the use of the equipment and truck since his work in the area was completed. We took data with the U.S.G.S. geode system recording 144 channels at 5m spacing. Vibroseis shotpoints were taken every 10m inside the linear profile and we took data from 3 additional shot points to the west and east of the array to obtain deeper refractions. 14-second data sweeps were recorded for each P wave vibroseis shot. After taking the P wave data, the geophones were switched from verticals to horizontals. An SH wave source consisting of a graduate student – powered sledge hammer hitting the end of a horizontal timber weighed down with the front end of a pickup truck was used to collect off-end and middle line refraction shots.

Duayne Rieger helped process the P wave data and pick SH wave traveltimes under a Mid America Earthquake Center Research Experience for Undergraduates position during the summer of 2007. Figure 2 shows a reflection image that he created from the P wave data. It is interesting to note that the prominent reflection at 650 ms is not the Paleozoic/Upper Cretaceous reflector that should be the largest velocity contrast interface at the site. Basement refractions seen in the large offset data suggest the basement occurs at a larger depth. This is consistent with what was seen in the 1982 U.S.G.S. Mississippi River profile where the basement reflector was rarely seen in the data. The P and S wave traveltimes from this data set were incorporated into modeling the K2 explosion waveform data (see below).

Because we had access to 8 PASSCAL CMG-40T broadband instruments with REFTEK data loggers after the 2002 experiment, we took the opportunity to install a broadband seismic array near the shotpoint to investigate ambient seismic background noise. The purpose of this was to collect data to characterize the source of the ambient

noise so that we could understand the wave propagation mechanisms important in controlling results obtained from the H/V method for determining site resonance and amplification. Figure 3 shows the the geometry of the array and Figure 4 the array response to various plane waves.

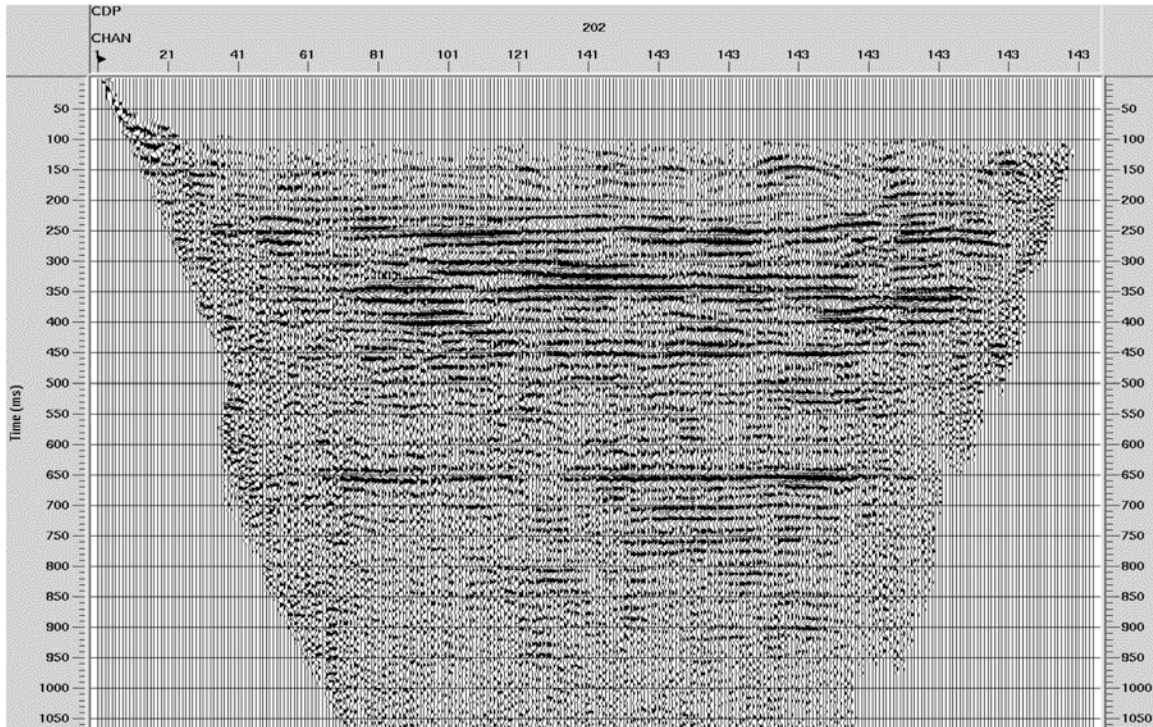


Figure 2 – Processed reflection data from the 16 November 2007 reflection profile at the Mooring site.

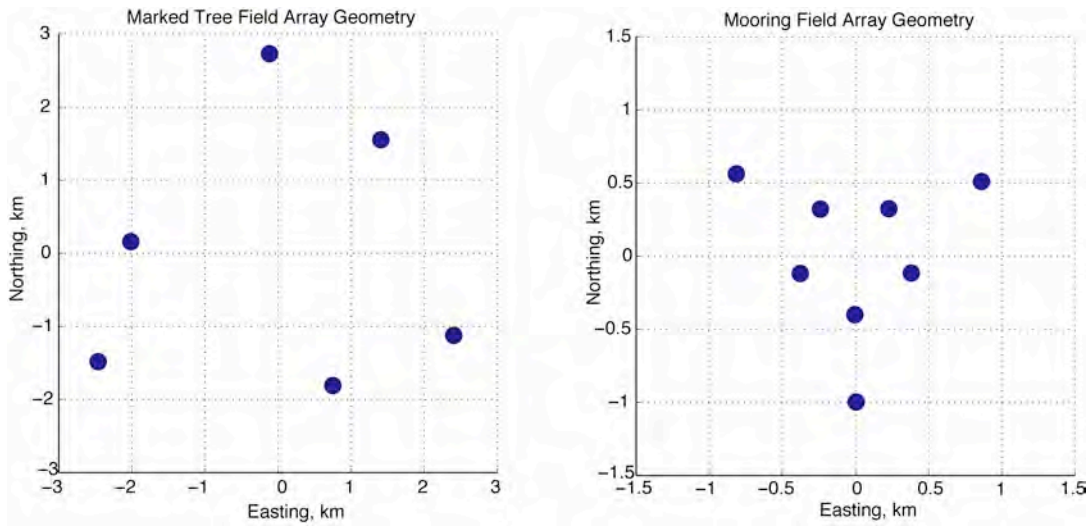


Figure 3 – Array geometries for the Marked Tree and Mooring broadband noise arrays.

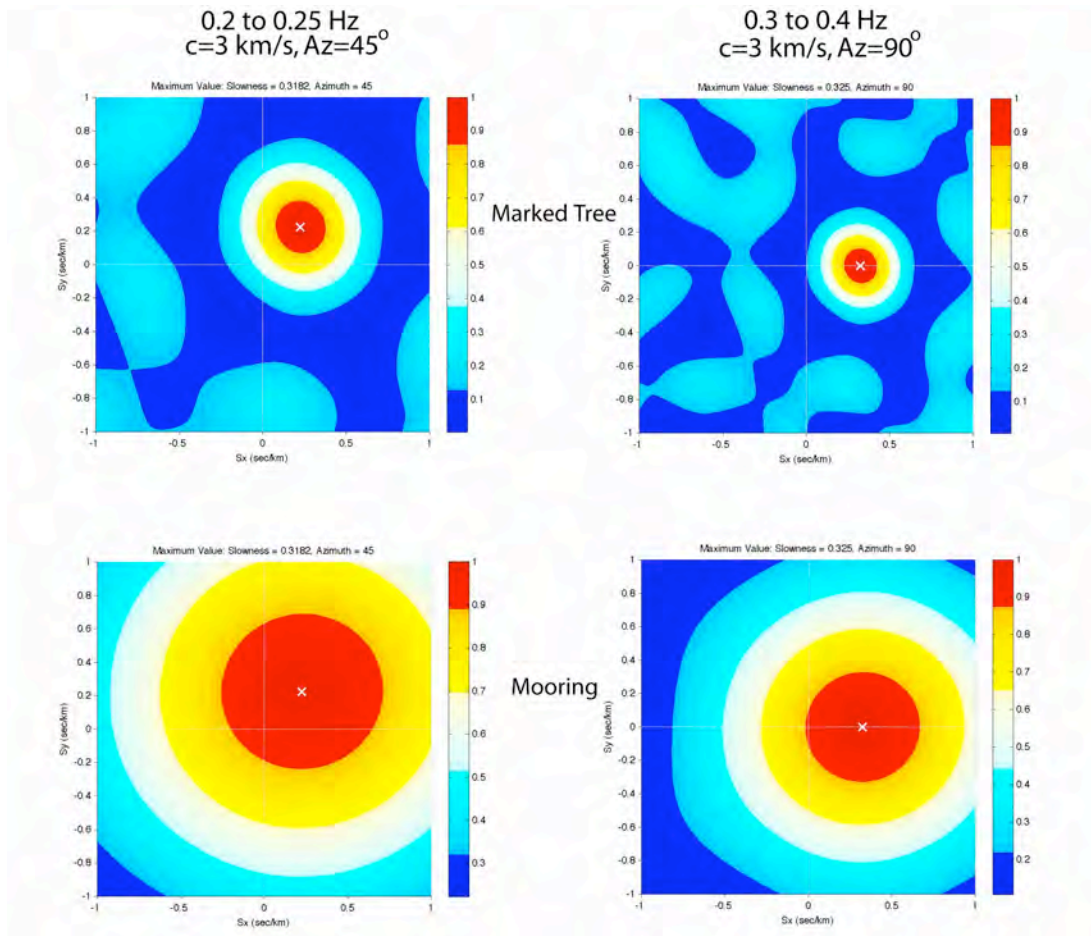


Figure 4 – Plane wave responses for the Marked Tree and Mooring arrays for 2 different plane waves showing the relative resolution.

The Mooring array was installed only for 1 night on November 26, 2002 to collect ambient noise data. The array was designed with a center element, but an animal chewed a wire early in the night that caused a malfunction. The Mooring array was designed to detect possible slowly propagating surface waves near the H/V peak period of 4 sec expected for the velocity and thickness of sediments in the area. However, the data showed that the ambient noise propagated at much faster velocity. The array response for a plane wave of 0.2-0.25 Hz propagating at the approximate observed velocity of 3 km/s is quite poor (Figure 4). Thus, the Mooring array could not be used to study ambient noise using standard frequency-wavenumber techniques. Since then, we have developed other high-resolution array techniques around the concepts of “wave gradiometry” [Langston, 2007a; b; c] that do allow a useful analysis of the wavefield. Results are discussed below.

Marked Tree Site

Figure 5 is an index map showing the environs of the Marked Tree site. This area is composed of large farm fields within the St. Francis River drainage system. The K2 array site and 2002 ESEE explosion shot point are separated by a large ditch of the drainage system that make the logistics of a long reflection/refraction profile somewhat of a problem. We chose to locate a 300m profile on the field road near the shot point using the 60 channel PASSCAL Geometrics StrataVisor system. The geophone interval was 5 m and we recorded 2-second length records. The source was a student-powered 16 lb sledgehammer impacting on a metal plate for the P wave source and the same hammer source hitting the end of the truck-loaded horizontal beam for the SH wave source.

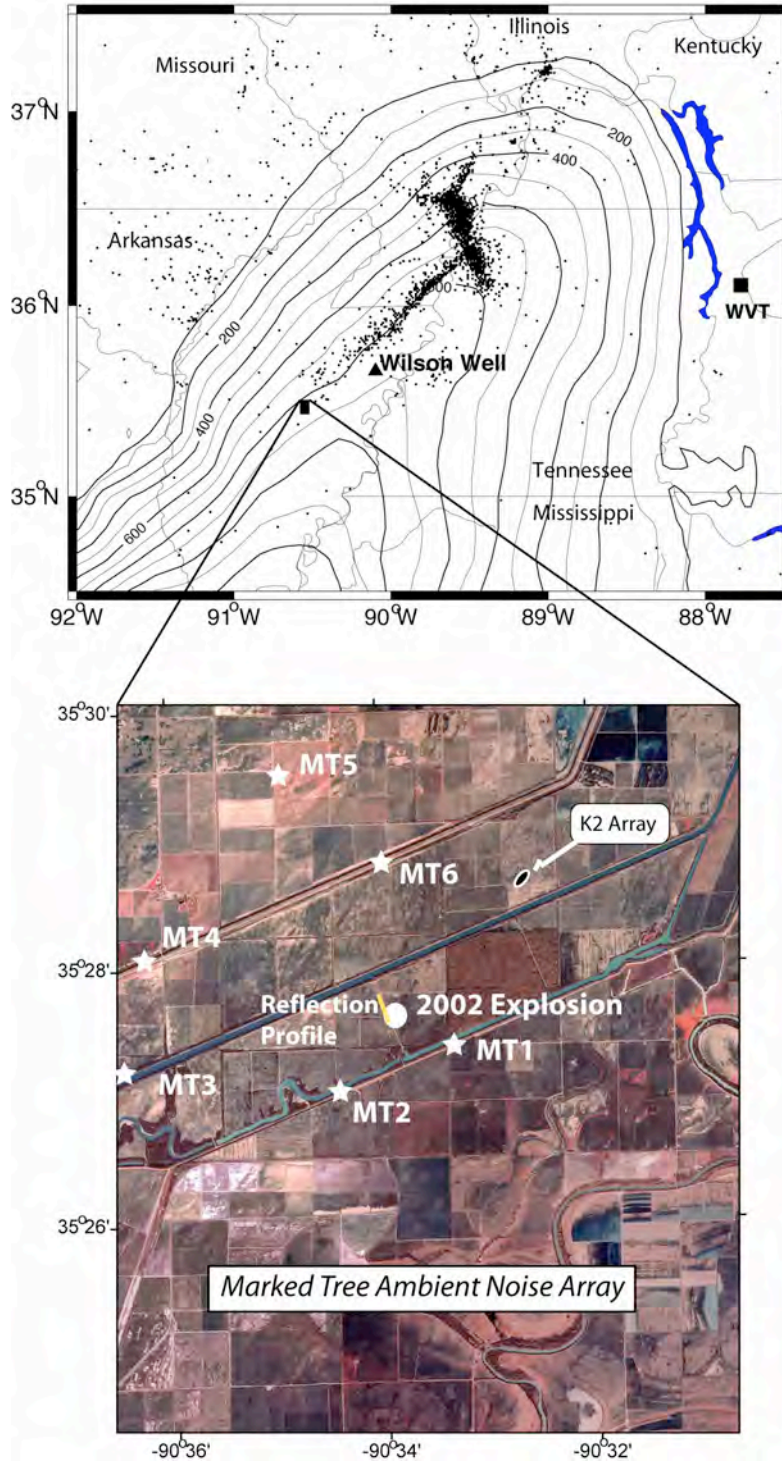


Figure 5 – Index map for the Marked Tree, AR, site. The shot point for the 2002 explosion and location of the strong motion K2 array are shown by the circle and ellipse, respectively. Stations of the broadband array experiment are shown by stars and the reflection profile by the short line next to the shot point.

A broadband array consisting of 6 three-component CMG-6TD portable seismometers was deployed in the area to collect microseismic ambient noise on 21-24 March 2007 (Figures 3 and 5). This array was designed to resolve the azimuth and slowness of 0.2-0.25 Hz microseisms that propagate at relatively high velocity, based on our experience obtained with the Mooring array. The array design was suggested by Fred Followill, a technical expert recently retired from the DOE, and was tested at smaller scale by a graduate seminar class at CERI in the Fall of 2006. Its principal characteristic is to sample the wavenumber plane evenly and without azimuthal distortion through the use of a minimum of seismic instruments. The ideal array response (Figure 4) for typical plane waves shows that its increased aperture (~4km) over the small Mooring array dramatically improves frequency-wavenumber resolution within the band of interest. The data were sampled at 100 Hz and all elements functioned for the duration of the experiment.

Non-Linear Wave Propagation Experiment at Blytheville, AR

We conducted a field experiment to investigate the *in situ* nonlinear properties of shallow soil deposits in the upper Mississippian Embayment. The experiment took place in the month of May, 2006, at “Joe’s Pond” near Blytheville, AR (coordinates N35.98177°, W089.91205°).

The Joe’s Pond site, located ~2 kilometers north of Blytheville, AR, was selected in part because of easy accessibility and a friendly land owner who has previously allowed numerous scientific field investigations on his land. The site also has paleo-liquefaction features at the surface. The liquefaction features are likely the result of past

large earthquakes along the southwest arm of the New Madrid Seismic Zone located only about a kilometer away. The Joe's Pond site lies adjacent to the Pemiscot Bayou, a tributary of the Mississippi River. The Pemiscot Bayou is a primary factor controlling the local soil content and plays a prominent role in the occurrence and nature of the paleo-liquefaction features exposed at the surface.

The liquefaction features at the Joe's Pond site serve as a stark reminder to the motivation behind investigating nonlinear response of near-surface soils in either the laboratory or in our case, in situ. Liquefaction is one of the severe consequences resulting from high-amplitude earthquake ground motions and is capable of causing considerable damage to man-made structures as well as putting lives at risk. Nonlinear response in the near-surface soils (or any material) is another way of saying the properties (i.e., the strength) of the soil is wave amplitude-dependent. Typically, soil strength decreases with increasing amplitude of excitation. Liquefaction represents an extreme case of nonlinearity, where permanent deformation occurs (as a result of high-amplitude excitation, the shear strength of the soil actually goes to zero as the pore pressure approaches the confining pressure). Nonlinear response similarly happens in a less destructive manner, yet sometimes with bad consequences to human-made structures. This is referred to as elastic nonlinear response, where the properties are temporarily affected by the high-amplitude excitation, yet without permanent structural damage. There exists a transition between when the soil's physical properties are unaffected by the amplitude of the passing seismic deformation (linear response) and when the soil temporarily weakens (i.e., elastic response, not permanent deformation). This transition, or threshold, is obviously different for different soils, although an accepted

approximation for all soils and rocks is near strains on the order of 10^{-6} . This experiment conducted at the Joe's Pond site, and other *in situ* nonlinear response studies we have conducted, focus on creating ground motions that will be near the typical threshold for nonlinear response.

The experiment at the Joe's Pond site utilized the Network for Earthquake Engineering (NEES) large mobile shaker truck named "Liquidator" to artificially create strong ground motions in the shallow soils. The strong ground motions were primarily restricted to a small area (< 10 meters) surrounding the shaker pad. The ground motions were recorded on an array of 13 surface-mounted 3-component accelerometers installed within 5 meters of the shaker truck.

Our field testing for *in situ* nonlinear response was designed to mimic the traditional methods of characterizing the linear and nonlinear soil properties conducted in a laboratory setting. Questions remain whether laboratory results reflect what happens *in situ* during large earthquakes. Simply analyzing strong ground motion records from large earthquakes for evidence of nonlinear response is a difficult and non-trivial task due to the complicated wave propagation and relative sparse occurrence of large earthquakes and existing strong motion networks. This has contributed to the motivation for creating the strong ground motions artificially in a controlled field experimental. The NEES shaker trucks allow us the ability to shake the ground at a wide range of applied force loads over a wide range of frequencies. We then can examine the observed wave propagation at the different applied force loads for evidence of any amplitude-dependent soil effects.

“Liquidator” is a large mobile shaker truck (Figure 6) owned by Network for Earthquake Engineering Simulation (NEES). It is considered their “low frequency” shaker truck, as it is designed to shake at controlled forces to lower frequency than the other two NEES shaker trucks; T-Rex, the 3-component truck, and “Thumper”, the high-frequency and low power truck, respectively. Theoretically, Liquidator can produce up to ~20,000 lbs of force (or ~90 kN) in a vertical orientation with controlled force loads between 1.3 and 75 Hz. However, during the experiment at the Joe’s Pond site, Liquidator reacted poorly to shaking at the lowest frequency limit, identified through audible sound and inspection of the ground motions records that show the noisy low-frequency waveforms. We decided not to shake below 5 Hz. Liquidator also has a mobile command center that staged in a sophisticated trailer that, along with the cab of Liquidator, has the ability to control the shaking operation and parameters.



Figure 6 – Liquidator and the experimental array setup at Joes Pond.

Adjacent to Liquidator we installed a 13 element array using 3-component strong motion accelerometers (Figures 6 and 7). The geometry of the array was designed

primarily for the analysis of wave propagation characteristics (i.e., wave velocity) across the array. The array consisted of 9 CERI K2 Kinematics 3-component accelerometers recording at 250 samples per second with +/- 4g of ground acceleration at full scale recording. These 9 accelerometers were installed in a linear array away from the middle of shaker pad with a nominal spacing of 0.5 m. The remaining 4 accelerometers were Episensor Kinematics Force Balance (FBA) 3-component accelerometers recording at +/- 2 g full scale. The Episensor FBA accelerometers did not have dedicated recording ability and the data from each one was recorded on one of the K2 accelerometers spare channels. The FBA accelerometers were installed to form a hexagon shaped sub-array next to the shaker pad. Data streams from Liquidator were also recorded with spare channels on one of the K2's. The Liquidator data streams included the theoretical drive signal and the estimated ground force output.

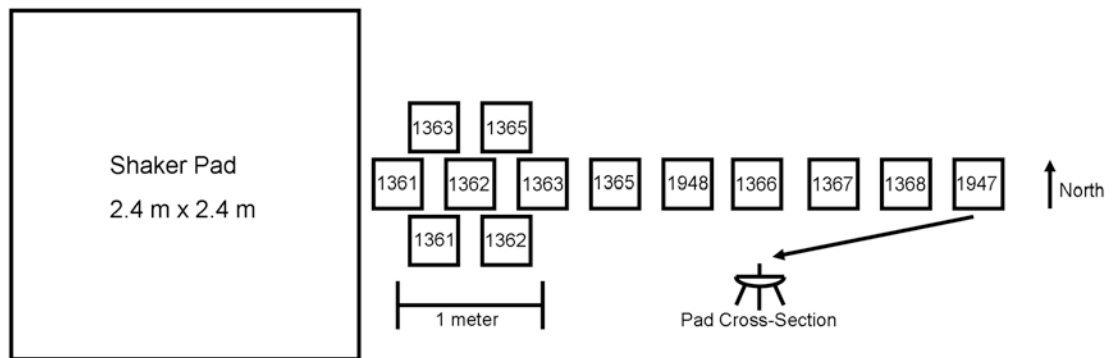


Figure 7 – Schematic of the strong motion array relative to the Vibroseis pad.

Due to the large ground motions created during the experiment, the accelerometers had to be tightly secured to ground. We secured the accelerometers to the ground by attaching them to a concrete pad, which was separately connected to the ground. This ensures that the concrete pad and, thus, the seismic instruments move in

sympathy with the passing seismic waves induced by Liquidator. The accelerometers were bolted to the concrete pad using a screw that was set in the concrete mass. The circular concrete instrument pads were ~20 cm in diameter and 5 cm deep. The concrete mass itself was securely attached to the ground using three 50 cm hollow metal tubes driven into the ground and set within the concrete (Figure 7). At the end of the experiment, the concrete pads were removed from the site. At that time, it was confirmed that the concrete pads remained intact and properly secured to the ground throughout the duration of the field experiment.

It was important to minimize the density contrast between the instrument pads and the low-velocity soil present at the site in order to decrease any unwanted effects in the seismic wave propagation across the array. This was accomplished by using a low-density, porous lava rock in the concrete mix. We allowed the concrete 25 days to fully cure before subjecting the area to the intense ground shaking. The cured density of the concrete was 2.11478 gm/cc (or 132 lbs/ft³).

Before nonlinear response testing, a site characterization survey was performed using a small sledgehammer and the CERI refraction seismograph. The site characterization was used to find a generalized subsurface velocity model for P and S waves and with particular attention to the depth of the primary seismic interfaces near the surface. The water table located at ~3 m was the primary P-wave interface. Above the water table the soil was extremely low velocity, with P-wave values less than the sound of speed in the air. The first major S-wave velocity interface occurred at ~9 m, since S-waves are not sensitive to the air-water difference at the water table interface.

SCIENTIFIC RESULTS

Blytheville Nonlinear Experiment

We conducted two days of nonlinear response testing at the Joe’s Pond site. The experiment was guided by two past field experiments involving *in situ* nonlinear response testing; one at Garner Valley, CA, and the other at Austin, TX, both using the NEES shaker truck “T-Rex”. Due to the unique nature of our field experiments, what field protocols we use – how we design the array geometry and how the details of how we use the truck to shake the ground – are in a constant state of flux as we determine the best way to setup and perform the experiment in the field. The Garner Valley experiment was our proof-of-concept experiment, our initial testing of ideas for this approach to nonlinear site characterization. One analysis approach using the Garner Valley dataset emerged involving the use of site resonance to identify and characterize the nonlinear response. The Austin, Texas experiment was a follow-up study using that analysis approach, with the array design and shaking protocols geared toward utilizing site resonance.

It was apparent, after an initial analysis, that a different approach of analyzing the initial Garner Valley dataset was more useful and versatile. Using wave propagation characteristics, particularly the wave velocity spectrum of high strain Rayleigh surface waves, nonlinear response could be quantified in a way more robust manner. The experiment in Blytheville was designed to primarily analyze the data for wave velocity changes as a function of applied force load. We refined the earlier Garner Valley methods and added new shaking protocols to answer questions that arose during the earlier Garner Valley analysis. Not surprisingly, pre-planning can sometimes be for naught because of difficulties in the field. This type of fieldwork uses a large, complex (and sometimes

cantankerous) machine that is integrated with an equally testy computer control vehicle. Field conditions and equipment problems during the experiment caused us to come up with *ad hoc* changes to the originally planned protocol.

The basic approach to our *in situ* nonlinear response testing is simple. We shake the ground at increasing applied force loads using the same signal for each force load (Figure 8). If the ground responds linearly, the same wave propagation characteristics should be observed for each different applied force load. If the ground responds nonlinearly (or with amplitude-dependence), the observed wave propagation will change, specifically the velocity of the seismic waves will slow down as the strength of the soil decreases due to the high strain deformations associated with the seismic wave field.

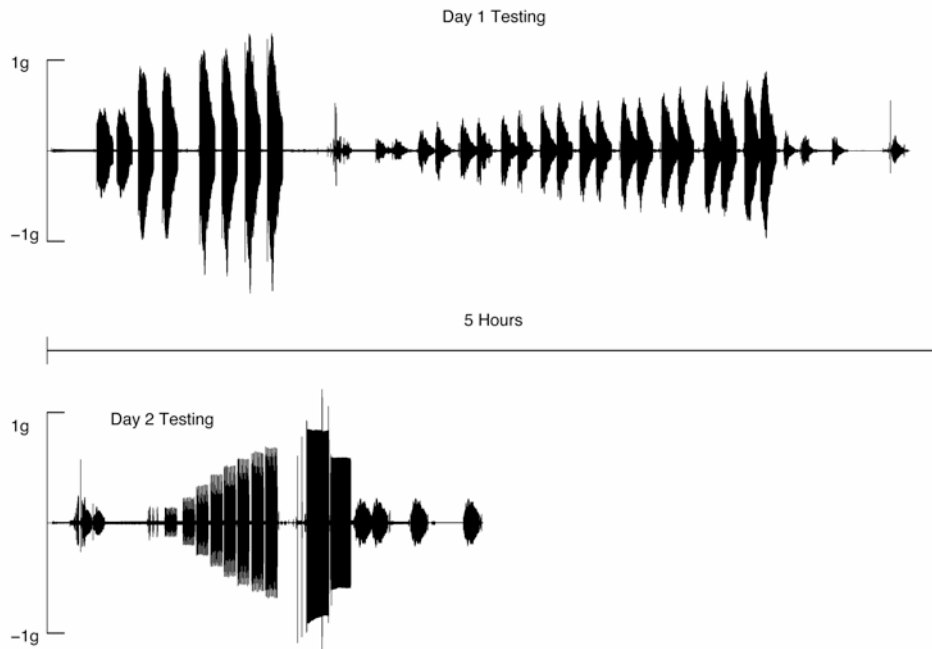


Figure 8 – Sweep signal protocol recorded by one accelerograph over the duration of the experiment.

Primarily we use a “sweep” signal during shaking (Figure 9). A sweep signal starts at one frequency value and progresses (either smoothly or discretely) through a range of frequencies. Our testing was also geared toward understanding the best type of sweep to use. We tried both a step sweep (discrete jumps between frequency intervals) and a chirp sweep (continuously changing frequency values). The step sweeps were much longer in duration than the chirp sweeps. We found both sweep signals produced the essentially same wave propagation characteristics and we preferred the chirp sweep to use during data analysis. The first day of testing was primarily focused on using step sweeps, while the second day was used for different signals such as the chirp sweep.

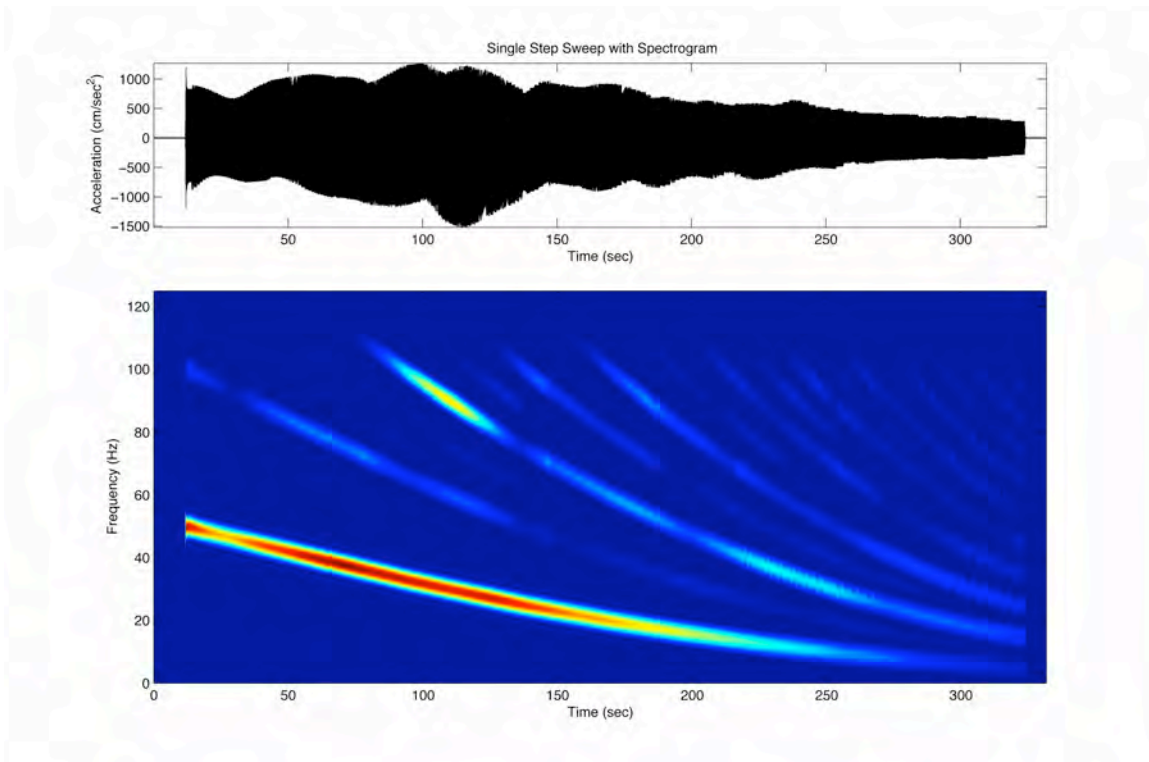


Figure 9 – Example of a sweep signal and its spectrogram showing the change in frequency with time.

The “bread and butter” of our analysis approach takes advantage of the type of seismic waves predominately created by Liquidator when shaking in a vertical motion.

Rayleigh waves dominate the wave propagation. This is evident by the retrograde elliptical particle motion observed in this and previous experiments. The sweep signals we use contain a range of frequencies. Surface waves of different frequency (and thus different wavelength) have different velocity values; this is called dispersion (Figure 10). We can calculate the dispersion spectrum across the array for our signals at different applied force loads. Therefore we can see not only the change in velocity as a function of force; we can see the change in velocity as a function of frequency (Figures 11 and 12). This surface wave dispersion spectrum can then be manipulated using simple, linear wave propagation models to invert for the S-wave velocity as a function of depth. This gives another look at the nonlinear response and allows for even more analysis, like the creation of shear modulus reduction curves, typically used in geotechnical engineering.

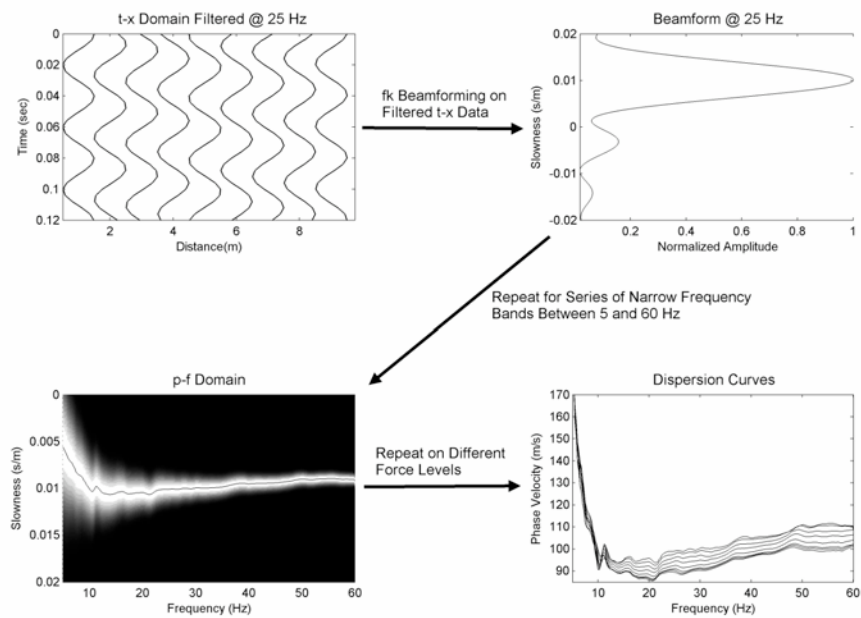


Figure 10 – Schematic of the process used to derive phase velocity dispersion curves as a function of frequency and force level. Filtered time series data are narrow-bandpass filtered and beamformed to estimate wave slowness. Inverse slowness is horizontal phase velocity.

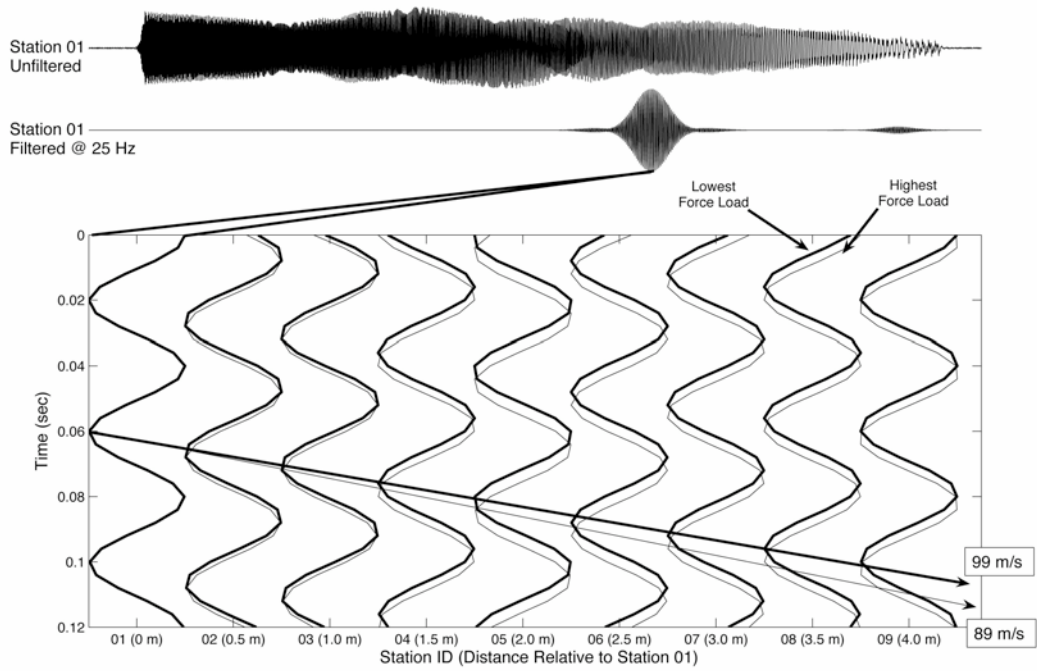


Figure 11 – Example showing the change in arrival time of peaks and troughs of a filtered Rayleigh wave propagating across the array at the lowest and highest force levels.

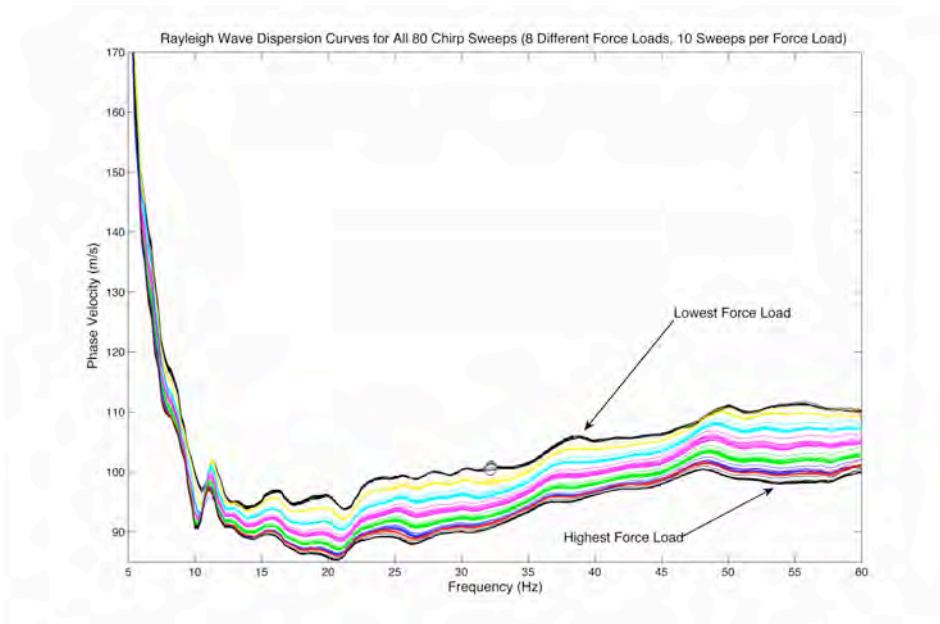


Figure 12 – Summary plot of the Rayleigh wave dispersions changes observed for all force loads. Phase velocity is observed to decrease with the force load implying nonlinear modulus degradation.

One question that kept arising when analyzing the Garner Valley data set involved the time dependent nature of the *in situ* nonlinear response being observed. We hoped to investigate the time dependence in this experiment in two ways. First, we shook at each force level multiple times. One observed characteristic of nonlinear elastic response in the laboratory is that when a material is subjected to repeated excitations at the same forcing level during a short time span, the material properties undergo “conditioning” and actually become weaker (Figure 13). Second, we investigated the “healing” phenomenon of nonlinear elastic response by quickly performing a refraction-like survey in between each applied force levels. Healing describes the process to which the material regains its strength after being driven to a nonlinear state (thus the term elastic nonlinear response). After shaking at a particular applied force load, we would hit a small sledgehammer on the side of Liquidator that contained the accelerometer array. Using a 24-element geophone array installed on the opposite side of Liquidator, we would record the seismic wave field produced from the sledgehammer. This way we could look use the velocity of the soil after shaking to determine how long it takes the soil to heal and regain its original strength. The geophone array only recorded the sledgehammer signals when Liquidator was not shaking.

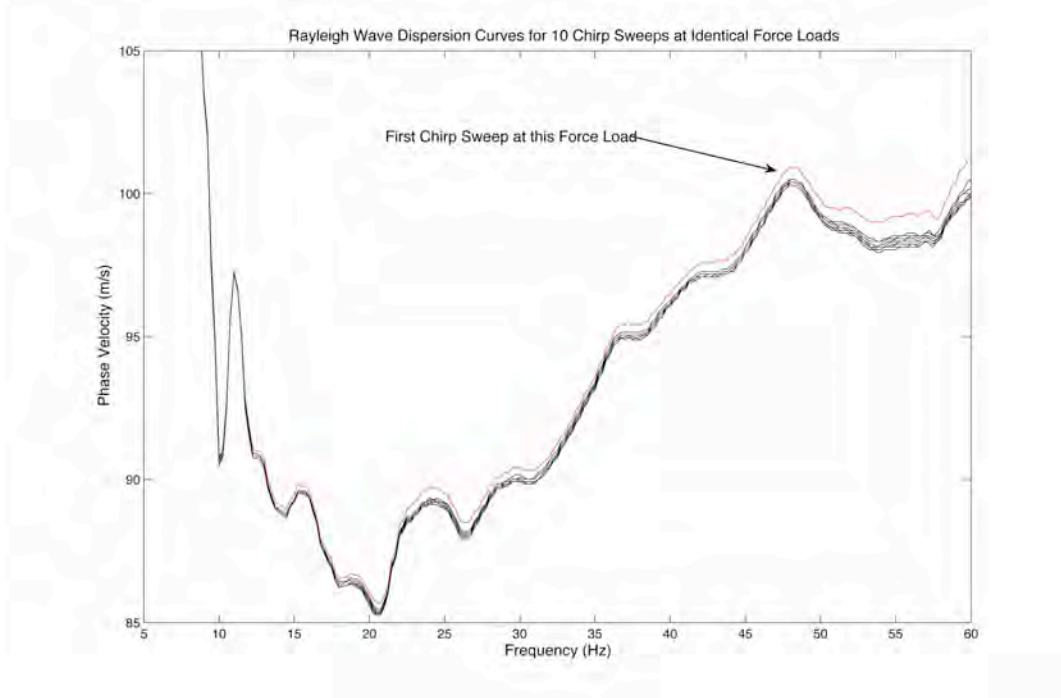


Figure 13 – Change in Raleigh wave dispersion under repeated, but constant, force loads.

Liquidator was able to create very strong ground motions in the vicinity around the shaker pad. Ground accelerations at the highest applied force load eclipsed 1 g. During large earthquakes, ground accelerations at as low as 0.1-0.2 g have been suggested to cause nonlinear response in the near-surface soils. The strains created by Liquidator were on the order of 10^{-4} , well beyond the cited threshold for nonlinear response in most geo-materials.

The data set is rich in information. We are just scratching the surface with our analysis. For instance, to go along with a velocity reduction in the wave propagation we should see an increase in attenuation. We are investigating ways to quantify changes in attenuation. One approach we are exploring uses the changes in the particle motion characteristics. In addition, we have more work to do inverting the calculated dispersion curves for S-wave velocity profiles, more accurately calculating the strain field, continue

investigating evidence for time-dependent nonlinear response, and look at the feasibility of applying new spatial gradient analysis on the data. This experiment forms part of a PhD thesis being written by Zack Lawrence.

Array Observations of Microseismic Noise and the Nature of H/V in the Mississippi Embayment

Nakamura's (1989) method for determining site resonance and amplification was used by *Bodin and Horton* (1999) and *Bodin et al.* (2001) to study these effects within the Mississippi embayment. The Mississippi embayment is a primary geological structure in the Central U.S. consisting of up to 1.5 km of unconsolidated upper Cretaceous to Recent coastal plain sediments (Figure 14). It has been the subject of intense study by a generation of seismologists and geophysicists because of the importance of unconsolidated sediments in amplifying strong ground motions from earthquakes in the New Madrid Seismic Zone (NMSZ). *Bodin and Horton* (1999) and *Bodin et al.*, (2001) measured ambient background seismic noise at various locations in the embayment and took spectral ratios of the average horizontal motion (H) to the vertical motion (V). They found that there was a significant correlation of the prominent H/V spectral ratio amplitude peak with known sediment thickness. Using the simple formula for constructive interference of a reverberating, vertical-incidence shear wave in a layer, they converted the observed frequency of the spectral peak into an estimate of average shear wave velocity (Figure 15). This is one of the few studies to systematically examine the

velocity structure throughout the embayment and is important in putting constraints on velocity structure essential to hazards computations.

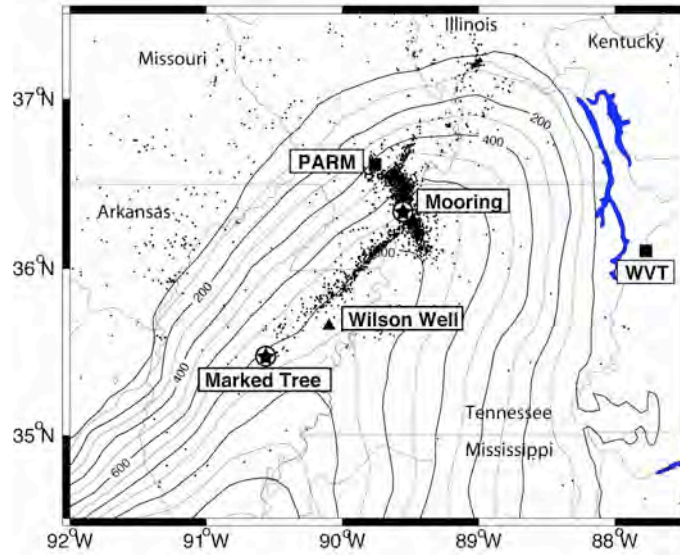


Figure 14 – Index map showing contours of unconsolidated sediment thickness, the locations of the Mooring and Marked Tree broadband arrays, PARM and WVT stations. The Wilson Well site is shown by the triangle. The contour interval is 100m.

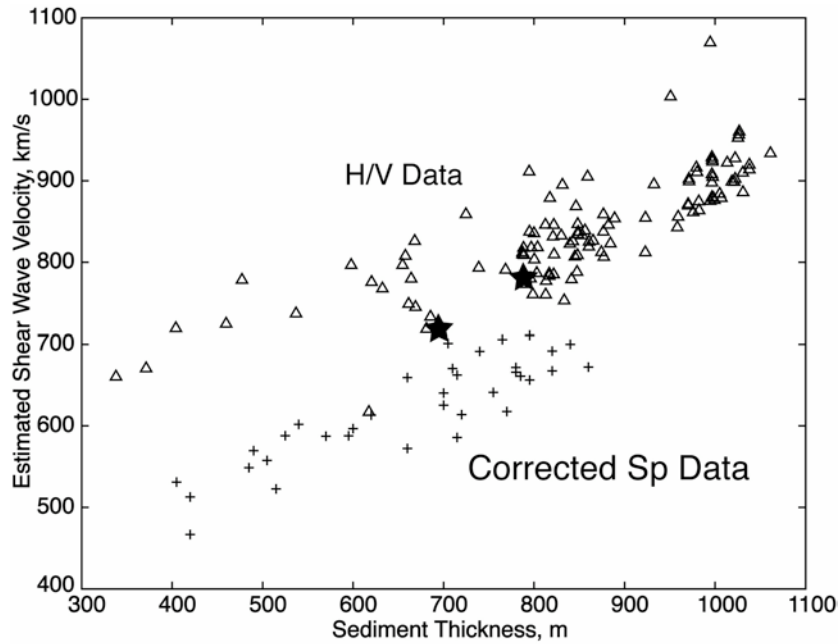


Figure 15 – Summary results from *Bodin et al.*, (2001) showing their estimates for shear wave velocity as a function of sediment thickness (triangles) using the Nakamura's method. The stars

show the location of results obtained from the broadband arrays. The plus signs are velocity-thickness estimates from S-Sp differential travel times measured from local earthquakes in the area by *Chen et al. (1996)*. The data sets are apparently inconsistent.

Figure 15 also shows a data set of S-Sp differential traveltimes measured from local earthquake seismograms that was used to estimate shear wave velocity by *Chen et al. (1996)*. The Sp conversion phase is one of the most prominent phases seen on local seismograms in the embayment because of the very large velocity contrast between high velocity Paleozoic dolomites just under the very low velocity unconsolidated sediments. Although both data sets show that average velocity increases with sediment thickness, the two trends are quite separate and inconsistent. There is a real problem here. On one hand, Nakamura's method is totally empirical. Although there is obviously a correlation of the H/V peak period with sediment thickness, there is no quantitative theory that robustly takes an unknown wavefield and produces spectral peaks. Is the simple plane wave model really true for ambient noise sources? Does the spectral peak in H/V represent a quantitative estimate of resonance and/or amplification due to the sediments? Are there biases in the velocity estimates using H/V? On the other hand, the S-Sp differential time data seems to be more firmly rooted in theory and practice. However, one might ask what Sp phase is really being measured. Could there be other interfaces that give rise to Sp phases that might be mistaken for the Sp from the unconsolidated sediments?

The object of our study was to take array measurements of ambient noise to understand what kind of waves propagate into the embayment and then to use this information to put constraints on the wave propagation mechanisms important in the amplification process. In other words, how does the H/V peak really form if the wave

types are known? Once the wave propagation mechanisms are known, what information on velocity (or thickness) does H/V really give? Is this information consistent with other data sets, i.e., the S-Sp differential times? Our objective is to thoroughly understand how the H/V method works in the embayment, what information does it really give, and whether this information is related to average sediment velocities of the unconsolidated sediments.

The H/V determination only needs one three-component observation of seismic noise. Our arrays (Figure 3) contain 6 to 8 individual elements that can be averaged to obtain average H and V spectra to form H/V ratios. Figure 16 shows H/V spectral ratios for the two arrays along with H,V, and H/V spectra for the station WVT. Data for WVT was obtained from the IRIS data center for the exact hour used to form similar spectra from the arrays. We chose data from 06:00 and 08:00 UT from the Marked Tree and Mooring arrays, respectively, since these time periods had no seismic events or other spurious noise signals, and were at times in the middle of the night where local cultural noise was at a minimum. Because the unconsolidated sediments of the embayment are so thick, the H/V peak is very close to the actual peak of ambient background noise. Figure 16 shows that WVT, a station situated on hard Paleozoic limestones has no H/V peak and that the H and V components are nearly identical for both hours. In contrast, the H/V amplitude peak attains a value of about 12 for Marked Tree at a period of 4.3 s and 8 for Mooring at a period of 4 sec. The spectra also show that the vertical component spectra largely remains the same whether inside or outside the embayment but that the horizontal component spectra becomes modified and amplified within the embayment. This is consistent with Nakamura's basic assumption on application of his method.

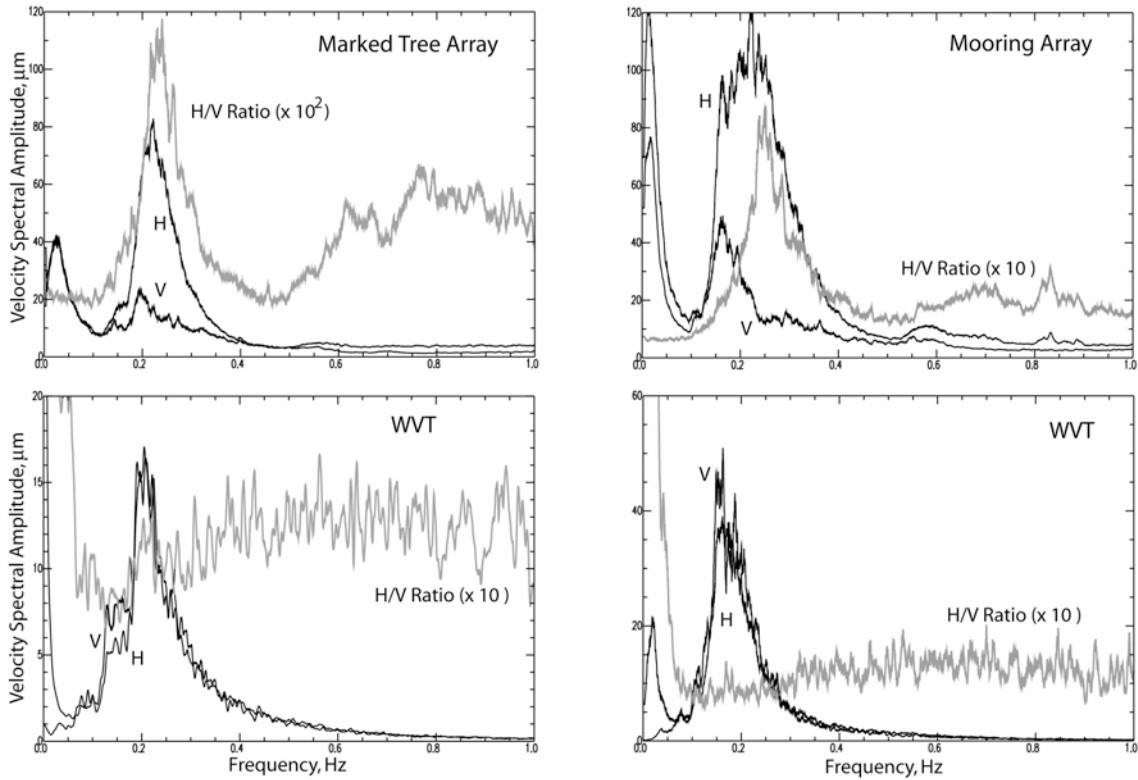


Figure 16 – Average H, V, and H/V spectra for the 2 arrays and WVT station for the same observation hours. Spectra for the NS and EW components from the arrays have been averaged to produce H and the vertical component spectra averaged to produce V. A smoothing operator was applied with a 20-point halfwidth to smooth the averaged spectra. The same process was applied to the three component data from WVT.

Using the Marked Tree array first, we investigated what waves contribute to the H/V spectral peak. Figure 17 shows narrow band frequency-wavenumber spectra for the Marked Tree data at the peak and to the right of the peak. The 0.2-0.25Hz result shows that the ambient noise field is highly correlated and consists of 3 – 4 km/s waves propagating from the northeast. The beam pattern is very close to the theoretical plane wave pattern shown in Figure 4 for the array and shows that a single harmonic plane wave fits the pattern well. Particle motion plots show that these waves contain both Rayleigh and Love waves. The result in the 0.3-0.4 Hz band is a little different. The

beam pattern is more smeared out indicating the contribution of waves propagating from northeast to eastern azimuths and with a variety of slownesses. The EW and NS components show relatively slow velocities of 1-2 km/s although the NS component also has a contribution near 4 km/s. The vertical component also shows reasonably high velocities of about 3.7 km/s. Thus, the ambient noise wave field is a mixture of coherent sources at low frequency and probably local/regional, more incoherent sources at slightly higher frequency.

We could not perform a frequency-wavenumber analysis of the Mooring array data because we under designed the array aperture. However, we have recently developed a new technique for analyzing wave fields using small, highly calibrated seismic arrays called wave gradiometry [*Langston, 2007c*]. Here, the array needs to be less than 10% of the seismic wavelength of interest so that spatial gradients of the wave field can be computed using finite differences of the data. Using the individual NS and EW array components from Mooring, we estimated azimuth from the spatial gradients and obtained a similar northeast source direction for ambient noise waves near the spectral H/V peak (Figure 18). Rotating the NS and EW components into an azimuth of 195 degrees, we then performed a waveform gradiometric analysis of a portion of the data to estimate wave slowness. For those waves that show peak motions and traveling close to the inferred wave direction (195 degrees), slowness estimates are similar to the Marked Tree result showing 3-4 km/s surface waves. Thus, results from both arrays show that the ambient noise wavefield near the H/V peak consists of 3-4 km/s Rayleigh and Love waves propagating from sources in the northeast at the time of observation.

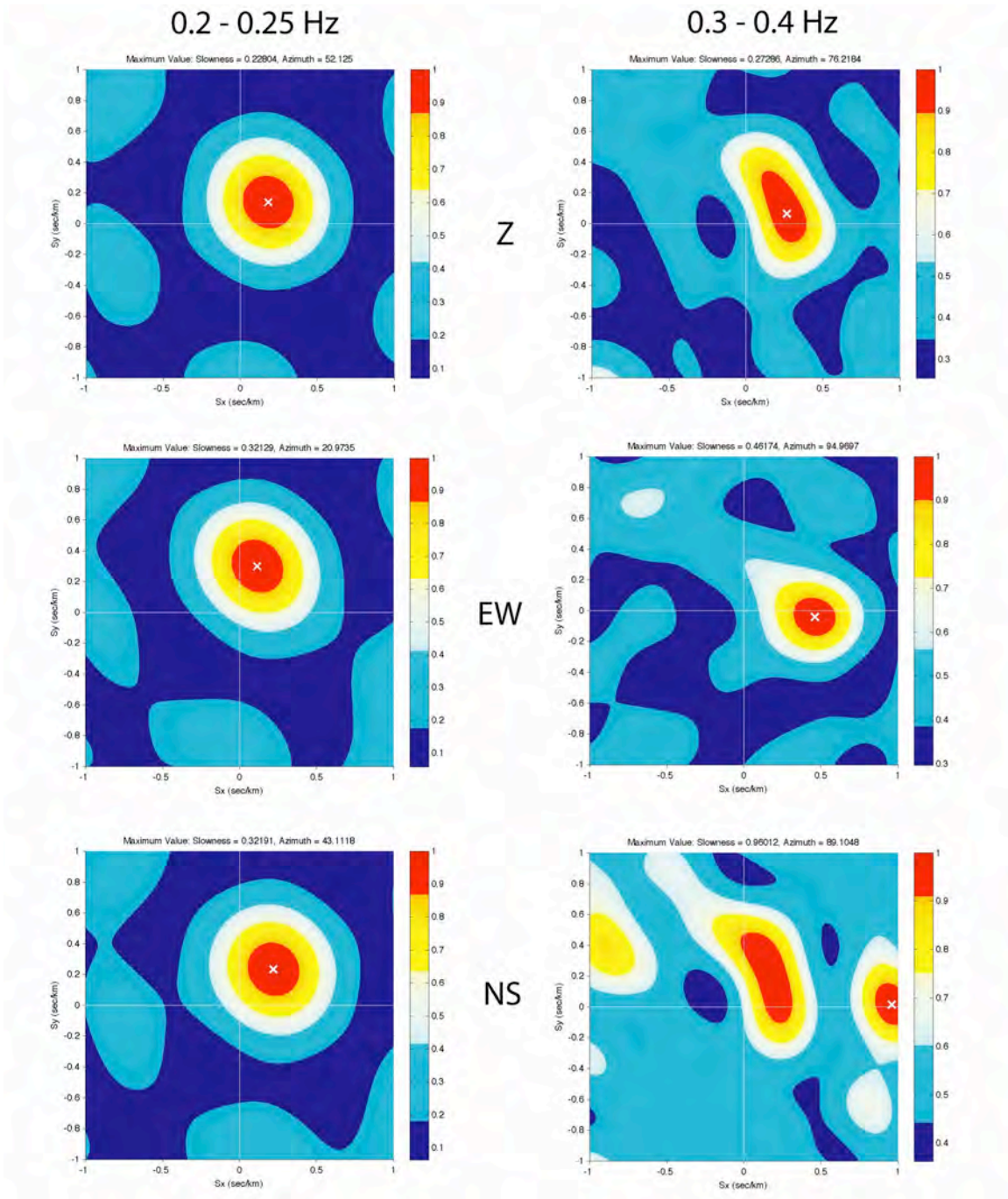


Figure 17 – Narrow band frequency wavenumber spectra for 2 frequency bands using the Marked Tree array data. Waves near the spectral H/V peak (0.2 – 0.25 Hz) are highly coherent and propagate from the northeast. They are 3-4 km/s propagating Love and Rayleigh waves. The wave field is less coherent at slightly higher frequency.

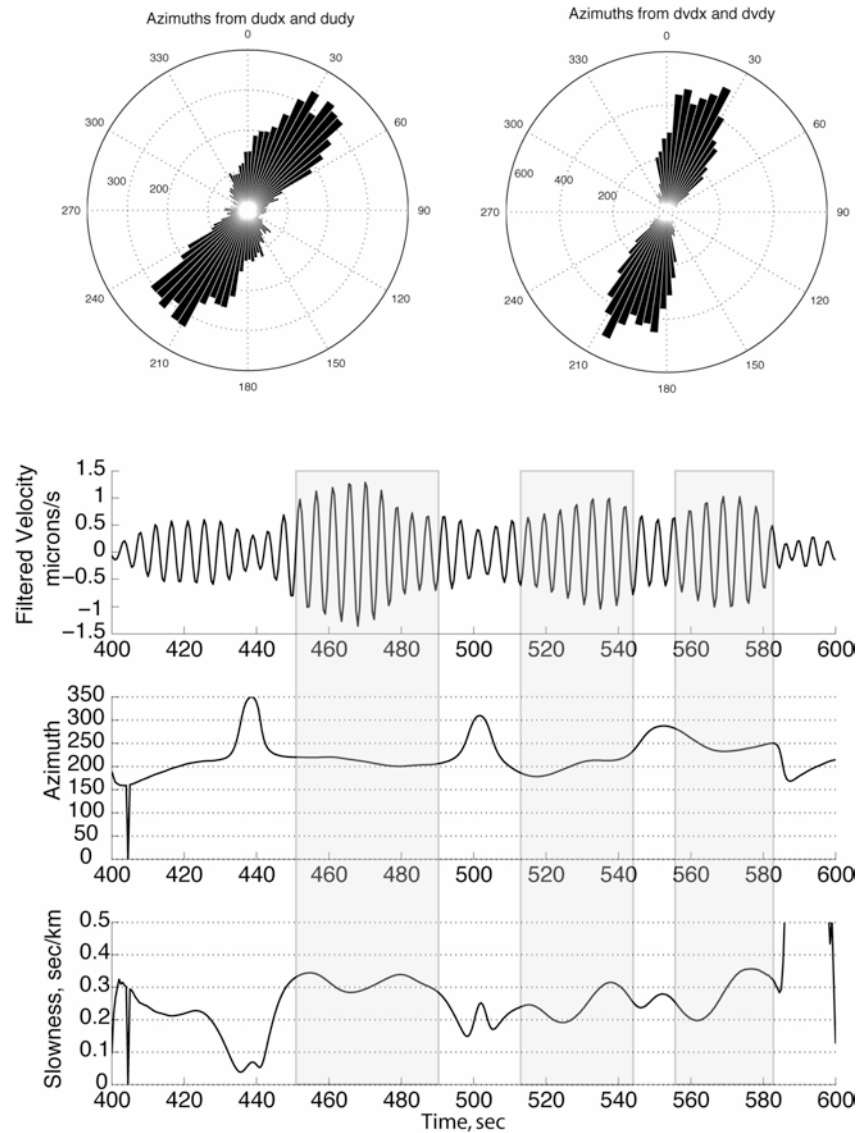


Figure 18 – Gradiometry analysis of data from the Mooring array. The upper rose diagrams show the frequency of azimuth estimates using the arctangent of the ratio of EW to NS spatial gradients. The distribution is similar to that seen in the frequency-wavenumber analysis of Marked Tree array data. The lower panel shows a gradiometric analysis of the rotated radial waveform using an azimuth of vector rotation of 195 degrees. The estimated azimuth is self consistent with the rotation showing that waves propagate from northeast to southwest – i.e., there is a source in the northeast. The inferred horizontal phase velocity for peak motions is 3-4 km/s, consistent again with Rayleigh waves.

The waves contributing to the H/V peak can be correlated with oceanic and meteorological data. Figure 19 shows a NOAA ocean wave height model built from wind and ocean buoy data for the array recording time periods. Large (>6 m) ocean wave heights were observed to occur in the North Atlantic and along the continental shelves of North America and Greenland. The microseismic background noise field is primarily due to nonlinear loading of the continental shelves by shallowing ocean waves [Bromirski *et al.*, 1999; Haubrich *et al.*, 1963; Longuet-Higgins, 1950]. The observed noise field at Mooring and Marked Tree is consistent with sources in this azimuth. Notably, there was no hint of sources to the northwest in the data. This may indicate that 4-5 sec surface wave propagation across the western tectonic zones of North America is highly inefficient. In summary, we now know, for these observations of H/V, the important parameters of the seismic waves that are affected by embayment sediments. What are the implications of these observations?

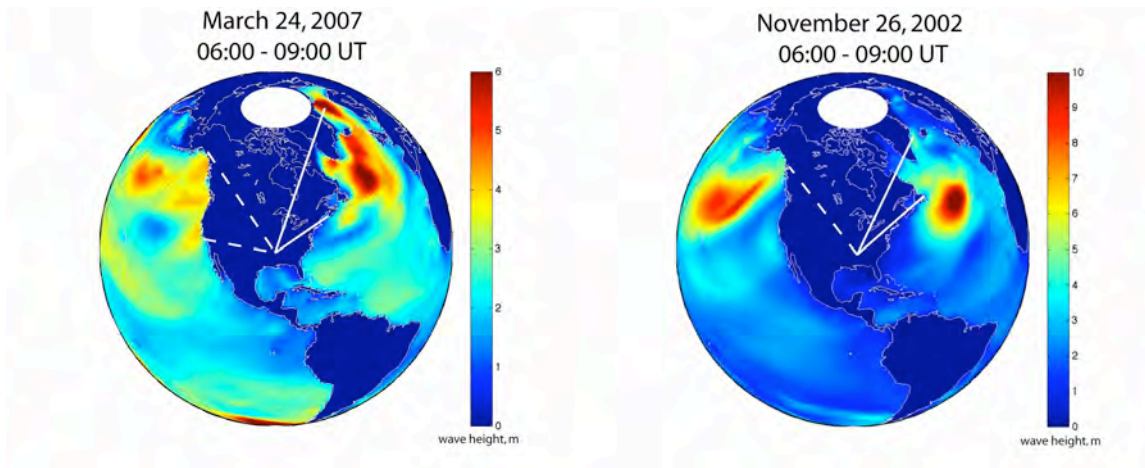


Figure 19 – NOAA ocean wave height models for the array observation time periods. Note the change in scale between the two images. High wave heights are seen in the North Atlantic along the North American and Greenland continental shelves. This is the source of the ambient noise field at H/V periods.

First, let's examine in more detail the nature of amplification of embayment sediments by forming the ratio of H and V spectra between each array and WVT station. In a sense, WVT is an ideal reference station since it is recording the ambient noise field just before it enters the embayment. Figure 20 shows H and V ratios of the data. The embayment tends to amplify both H and V above 0.4 Hz. Notably, the V curve shows that very little happens to vertical motions near 0.2-0.25 Hz as these waves propagate into the embayment. *Konno and Ohmachi (1998)*, *Lachet and Bard (1994)*, and *Lermo and Chavez-Garcia (1994)* suggested that the H/V peak was controlled by a Rayleigh wave ellipticity null in frequency. These data show that the vertical component has no null relative to a non-sediment reference station and so the ellipticity argument does not apply to these data.

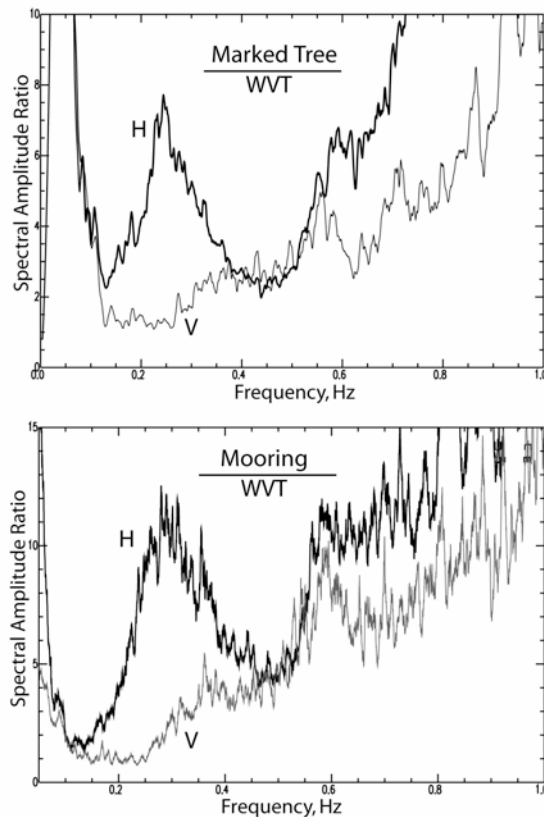


Figure 20 – Ratios of H and V spectra between the arrays and WVT station.

High velocity 0.2 to 0.25 Hz surface waves have a vertical wavelength of roughly 15 km. However, the average shear wave velocity of unconsolidated sediments is so low, ~ 0.7 km/s, that these high velocity, horizontally propagating surface waves must convert into near-vertically propagating shear body waves at the base of the sediments just because of the requirement of matching the horizontal phase velocity at that boundary. Thus, we can gain some insight on the wave propagation mechanisms by examining a realistic velocity model for the unconsolidated sediments using appropriate input phase velocities and a plane wave propagation model.

Figure 21 is a compilation of synthetic H peaks assuming input SV and SH plane waves with slownesses between 3 to 10 km/s. We formed the ratio of the horizontal response of an S plane wave for the layered structure to that from a halfspace. The velocity model (Figure 22) is based on the interpretation of two acoustic velocity logs from the Wilson Well site (Figure 14). The detail of the model is not needed to model the H peaks but is included to show that the sub-unconsolidated sediment structure is high velocity and similar to that under WVT station. We took the unconsolidated sediments above as the model and set the lower structure as a simple halfspace. Figure 20 shows that the position of the H peak depends on wave type (incident SH or SV) and slowness. Indeed, the spectral peak is a complex function of Rayleigh or Love wave dispersion in the unconsolidated sediments for slowly propagating waves (< 3 km/s) but settles down to a consistent value for high velocity waves that is expected from the simple plane wave expression for resonance:

$$T = \frac{4h}{v} \quad , \quad (1)$$

where T is the period of the H peak, h is the layer thickness, and v the average shear wave velocity. Thus, we conclude that the H peak can be understood from the simplest viewpoint – that of near-vertically propagating shear waves in the layer. Based on our observations of the spectra between the arrays and WVT station, the H/V ratio simply removes the common effective source time function since the V spectra are largely unchanged as these waves propagate into the embayment.

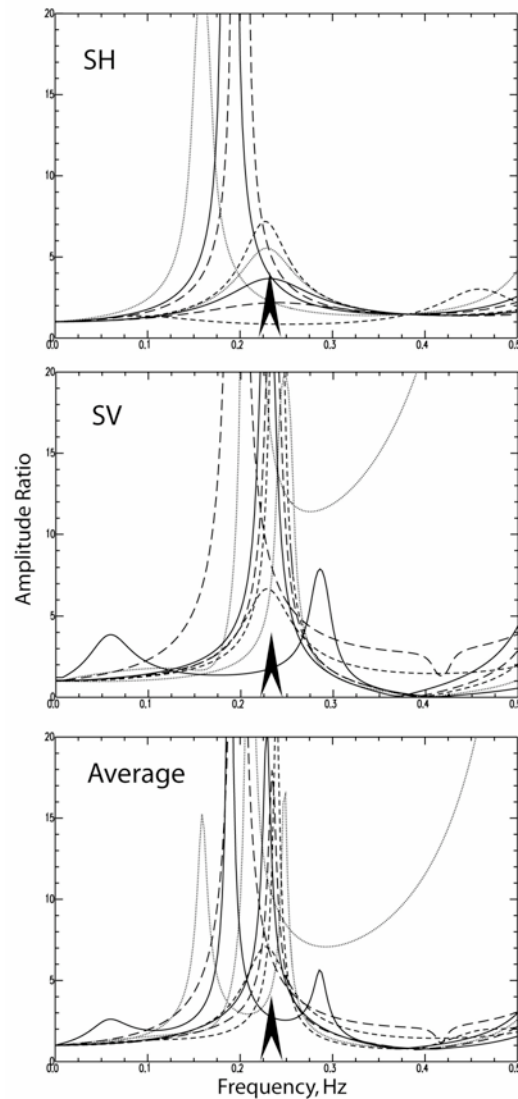


Figure 21 – Synthetic transfer functions for incident SV and SH waves. The ratio of responses from the unconsolidated sediments to that of a halfspace are shown. The “average” curves are

averages of the SV and SH transfer functions. The arrow shows the expected position of the H peak assuming vertical S wave propagation.

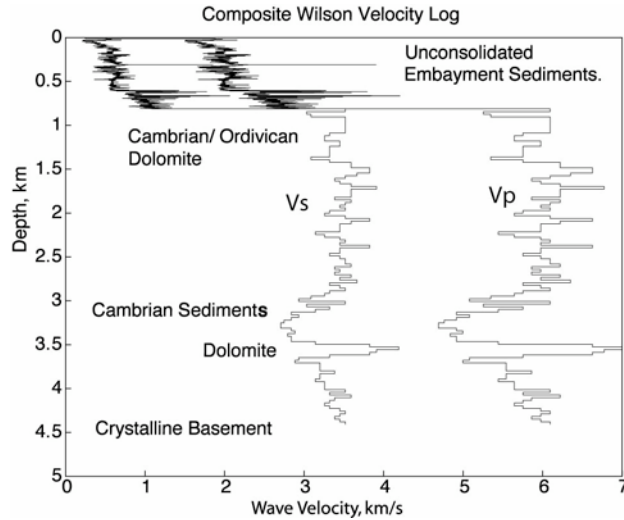


Figure 22 – Velocity models derived from the Dow Wilson #1 well and Wilson 2-14 well acoustic velocity logs. Shear wave velocity was derived from a sediment model [Langston, 2003].

We conclude that the H/V data shown in Figure 15 are giving a reasonable approximation of the average shear wave velocity structure of the embayment. However, the transfer functions of Figure 21 imply that amplification will be a function of the incident wave type and slowness. We expect that the amplitude of the H/V peak could change with time depending on the slowness of ambient noise waves. For example, waves propagating up from the Gulf of Mexico during times of high storm surf might be dominated by Rayleigh and Love waves slowly propagating exclusively within the unconsolidated sediments. These sources might show a lower frequency H/V peak or could be a function of the ellipticity null as postulated by others. The amplification factor of 8-12 seen here is due primarily to having the reverberating shear body waves locked into the unconsolidated layer because the incident waves are horizontally propagating.

Shear waves from a local earthquake source will have faster horizontal phase velocities and, hence, would not become locked into the layer displaying lower spectral amplifications.

These leaves the final detail of understanding the difference between the velocities inferred from H/V and the Sp differential times. Research unrelated to this project (Chiu, personal communication 2008) is showing that the Sp data have probably been misinterpreted. Figure 23 shows that the Sp arrivals from local earthquakes is often complex. For example, using the average velocity of unconsolidated embayment sediments and thickness derived from well log and seismic reflection data (Figure 14), broadband data show distinct Sp phases at the correct arrival time but that there are clear precursors that imply deeper interfaces (e.g., see *Langston [2003]*). Thus, using the first Sp arrival as the Sp from the unconsolidated sediment interface biases the differential S-Sp time. The larger inferred time produces a slower velocity for an assumed depth of sediments. The effect can explain the nearly factor of 2 in the inferred sediment velocity.

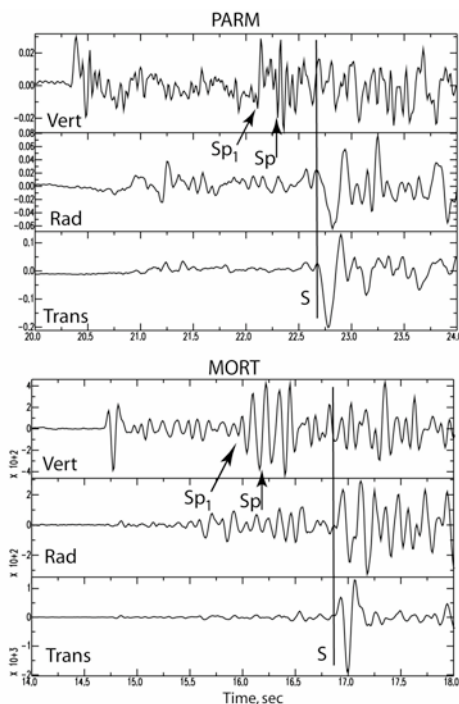


Figure 23 – Local earthquake seismograms rotated into vertical, radial, and transverse directions with S and Sp phases annotated. MORT is located within 2 km of the Mooring blast site and PARM in a shallower part of the embayment (see Figure 14). The expected Sp phase from the unconsolidated sediment boundary is shown by Sp. Sp1 is where one might pick the arrival time of the entire Sp wavetrain. Sp1 is inferred to originate at a deeper interface within the Paleozoic sedimentary rocks.

Possible Non-volcanic Tremor Discovered in the Reelfoot Fault Zone, Northern Tennessee

One of the most exciting discoveries to be made within the NMSZ in recent years is the possibility that non-volcanic tremor may be occurring on the Reelfoot fault. Non-volcanic tremor is an awkward name for a relatively new phenomenon in fault dynamics. Non-volcanic tremor has been found to be associated with episodic slip episodes in the Cascadia subduction zone of the Pacific Northwest where elevated levels of microseismic activity occurs during periods of slow slip on the subducting plate interface below the locked, seismogenic zone [Brudzinski and Allen, 2007; Dragert et al., 2001]. This activity occurs as a continuous background level of motion punctuated by periods of earthquake event-like bursts that may be occurring on the plate interface or in the crustal wedge above [Rogers and Dragert, 2003]. Non-volcanic tremor occurs in tandem with GPS signals indicating slow slip on the plate interface in Cascadia but may also occur without any clear GPS signal in the subduction zones of Japan and Mexico [Schwartz and Rokosky, 2007]. Non-volcanic tremor has also been observed at deep levels of the San Andreas fault in central California as clusters of events in an elevated level of microseismic background activity [Nadeau and Dolenc, 2005]. There is no consensus to what this phenomenon means or to its mechanism. However, it appears to be related to visco-elastic and chemical processes in deep levels of fault zones that indicate active motion within the fault system. Non-volcanic tremor is difficult to study because source areas appear to be spatially distributed and seismic radiation is continuous in time.

Figure 24 is a repeat of the index map showing the location of the 16 November 2006 reflection experiment in the Mooring, TN, area in relation to located instrumental seismicity.

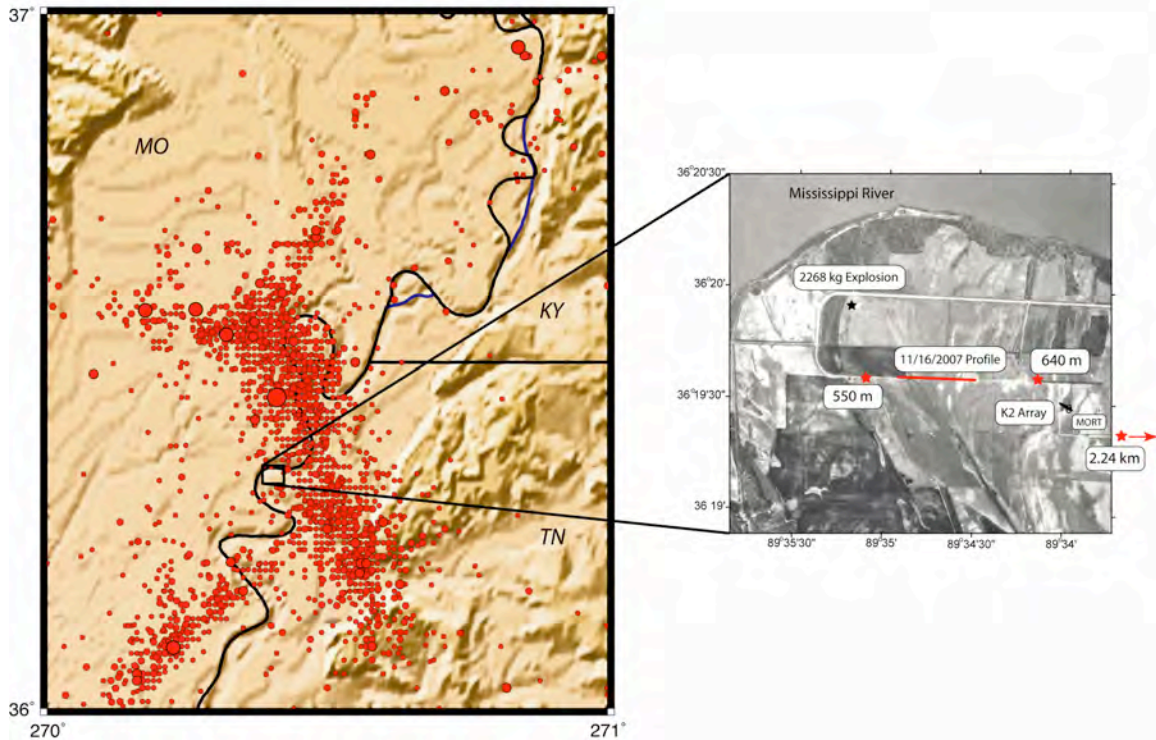


Figure 23 – Seismicity in the vicinity of the Mooring, TN, area. The image to the right shows the geometry of shotpoints and location of reflection profile.

Three far-offset vibroseis shot points were occupied to provide longer distances to pick up the basement refraction. They were located 550m west of the line, 640m and 2240m east of the line. Because the vibroseis source was outside of the line, signal levels were low and the 14 s time recording allowed a significant amount of background ground motion to be recorded. While processing the data during the summer of 2007, we noticed some unusual “events” or “reflectors” within the CDP gathers for these far-offset data that did not make sense. Indeed, every original shot gather for the far-offset data showed

high-velocity arrivals after filtering that could only mean that we were recording deeper seismic activity. For example, Figure 24 shows an example shot gather with a near-continuous set of high velocity arrivals sweeping across it.

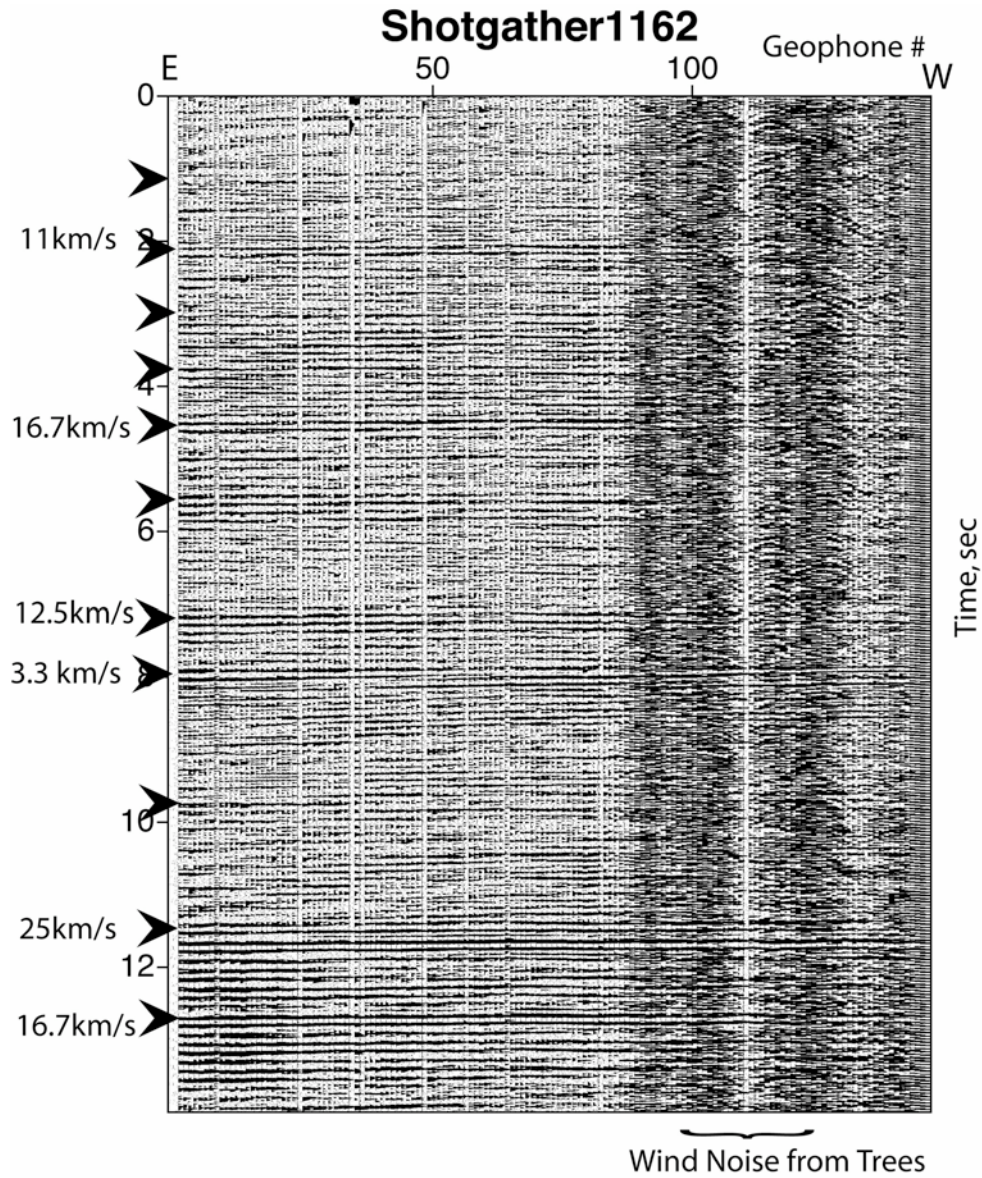


Figure 24 – Example far-offset vertical component shot gather filtered between 3-30 Hz. There are numerous high velocity arrivals sweeping across the array with differing horizontal phase velocities. The dark area to the right is due to wind noise from trees adjacent to the profile.

All 20 far-offset shot gathers showed high velocity arrivals and all arrivals had a component of moveout that indicated that the causative events were located west of the array. We considered all possible sources of noise that might be observed during that afternoon including possible signals from barge traffic on the Mississippi River, local well pumping sources, or vehicular traffic. However, the relatively impulsive nature of the arrivals, high phase velocities, and coherence across the array suggests earthquake-like sources greater than 5 km from the line. Some events had curved wave fronts and suggested that they occurred either directly under the array or nearly perpendicular to it to the north or south. The amount of curvature is consistent with source distances of 5 km or more. The dominant frequency of the events is 10-20 Hz.

Using the nominal response of the Geode seismograph and the response of the 8Hz vertical geophones, we corrected the reflection shot gather data to ground displacement and then convolved the result with the nominal Wood-Anderson seismograph response. This was done to give us estimates of the ground motion that could be used to infer possible local magnitudes for the events and for comparing to similarly corrected seismic data from the nearby CERI station MORT (Figure 23).

Figure 25 shows an example local earthquake record from MORT station. Events within the NMSZ show characteristic Sp conversions on the vertical components of motion due to the large velocity contrast at the Paleozoic/Upper Cretaceous interface, here about 700 m under the station. There are also large secondary reflections and conversions within the vertical waveforms that generally give a complex, long-duration signature (e.g., *Langston* [2003]). Compare this figure with Figure 26 that shows 4 different shot traces from geophone 50. The larger double arrivals seen in the shot gather

data are similar to the Sp converted phases seen in the earthquake data. Vertical waveforms seen at MORT station from local earthquakes show a large amount of variability depending on the relative radiation patterns of P and S waves. However, the similarity in frequency content and wave shape character between the shot gathers and MORT data suggest that we are observing a series of very small earthquakes in the reflection data.

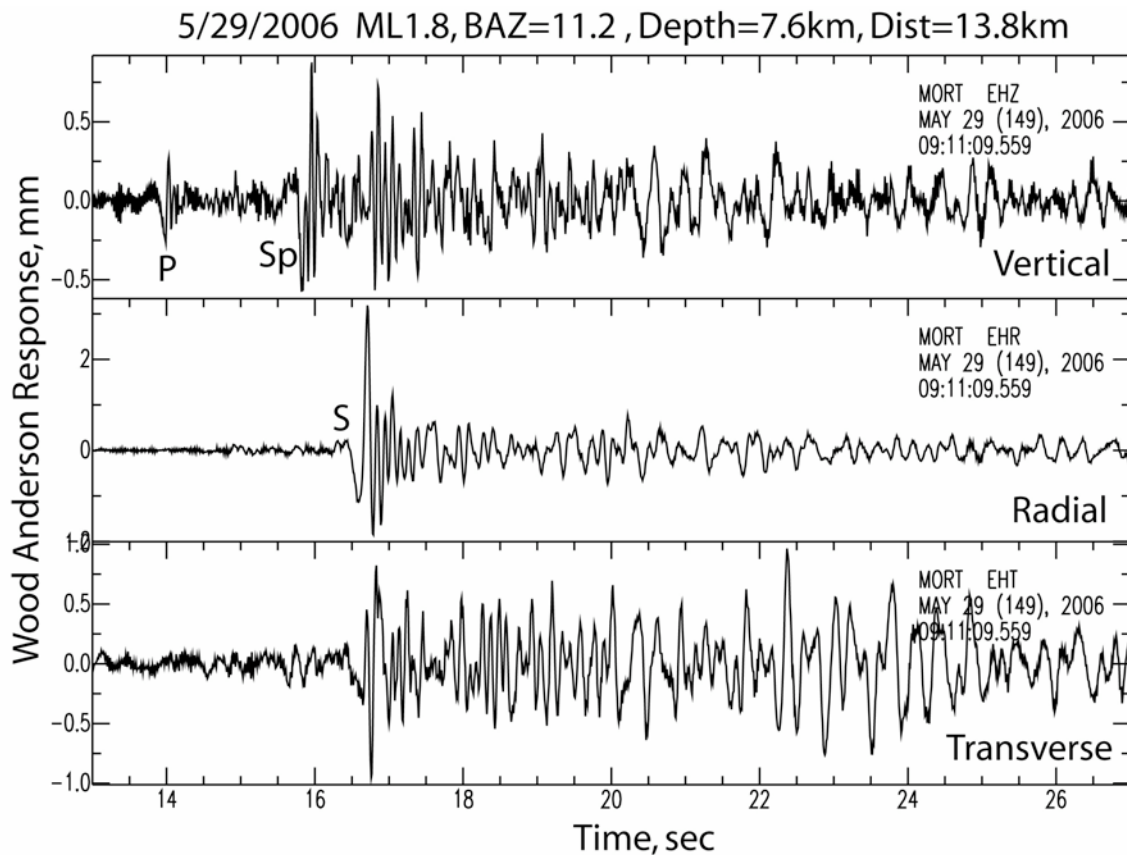


Figure 25 – Example of a small, local microearthquake recorded at MORT station. The 3 component data have been corrected to ground displacement and convolved with the nominal Wood-Anderson seismograph response. Note the large Sp conversion seen on the vertical component of motion caused by phase conversion at the Paleozoic/Upper Cretaceous interface under the station. The vertical waveform consists of a long train of the converted, reflected and scattered phases. Also note that 14 sec of data are shown, consistent with the recording time of the vibroseis data in the reflection profile.

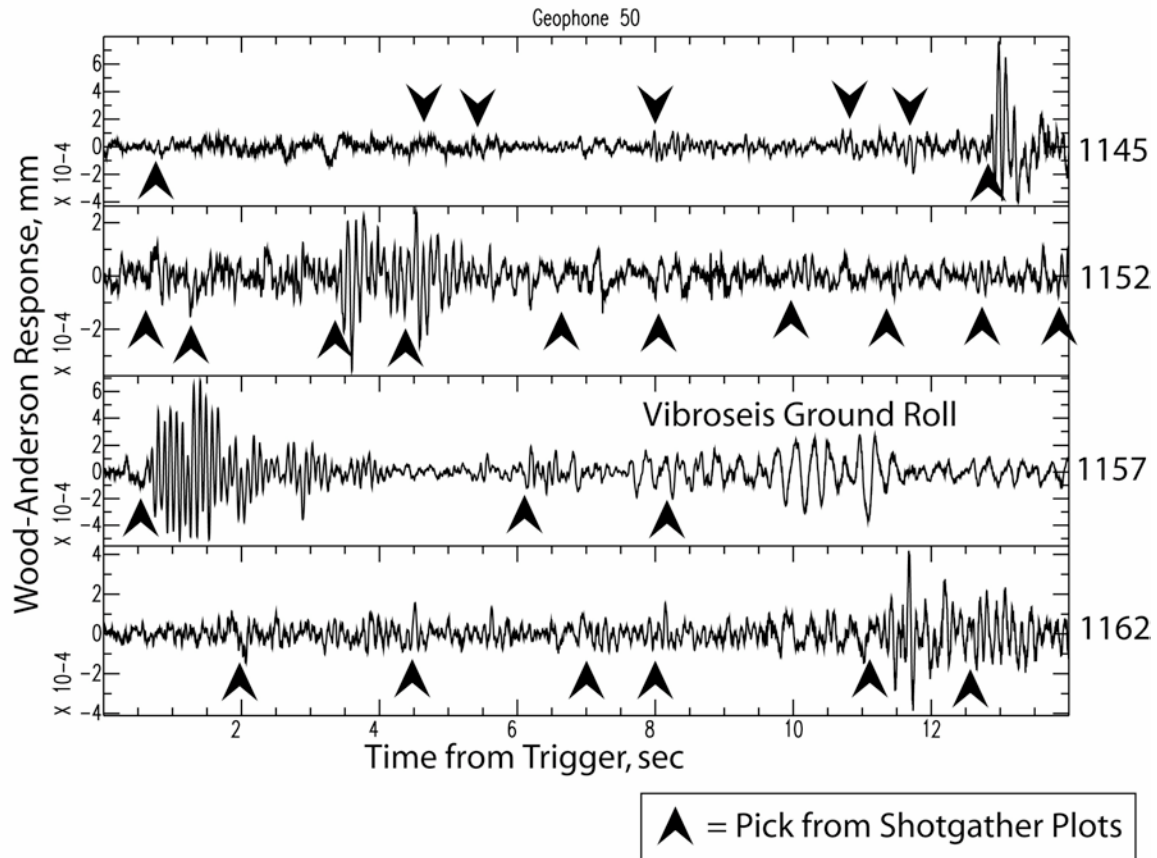


Figure 26 – Five different shot records from geophone 50. The data have been corrected to the nominal Wood-Anderson instrument response. The arrows show the time locations of clear high-velocity events seen in each shot gather. The larger phases seen in these data traces are similar to the Sp conversions seen from local earthquake data (e.g., Figure 25). Under this interpretation, the smaller amplitude phases could be later arriving reflections and scatter waves or Sp or P waves from smaller events.

There are numerous high-velocity arrivals in the large offset shot gathers that range in velocity from 3.0 to 25 km/s. The variation suggests diverse locations for the source of the waves and the low velocity end is consistent with the expected slowness for Sp converted phases. We stress converted phases because vertical component data from stations in the NMSZ are dominated by P-type waves due to the thick, unconsolidated low velocity sediments that blanket the area. There are 20 large offset shot gathers and

all show high velocity events. The data at MORT suggests that one microearthquake could give rise to many secondary “reflection” events over the 14 sec time duration of a shot record. Therefore, we estimate that there could be as little as 20 separate events for all shot gathers or as many as 80 if smaller events come from separate source areas. Each shot was separated in time by as much as several minutes when the vibroseis moved but usually by about a minute when the source was at a single shot point. 4.7 minutes total amount of time were recorded by each shot record during the hour or so it took the vibroseis source to drive around on that afternoon in the field. The density of events seen in the shot records suggests that events were occurring continuously throughout the time period. This gives a remarkable seismicity rate of 257 to 1029 events per hour.

The approximate size of the events can be estimated 2 ways from the corrected ground motions. First, the maximum ground motions seen in the reflection array data are 2 to 3 orders of magnitude smaller than the smallest earthquakes recorded by the CERI network or MORT station (e.g., compare Figures 25 and 26). This yields events in the M_L -1 to -2 range considering that the smallest earthquakes seen at MORT are in the M_L 1.5 to 1.8 range. We obtain the same M_L estimates if we use the maximum observed ground motions and assume that the event distance is 5 to 10 km from the reflection line by using a recently derived local magnitude scale for the NMSZ [*Miao and Langston, 2007*]. *Miao and Langston (2007)* also derived the background seismicity rate using a Gutenberg-Richter relation and obtained

$$\text{Log } N = 3.2 - 0.79M_L \quad . \quad (2)$$

This relation gives $N=1.1$ / hour for M_L of -1 or greater and $N=6.9$ /hour for M_L of -2 or greater. If the earthquakes are farther away than 10 km then the events must be larger

and the expected seismicity rate must be smaller by relation (2). The events cannot be larger than about $M_L 1.5$, the magnitude threshold for detection by the CERI network. By any measure, then, we have detected an unusually energetic earthquake swarm of very small events in the NMSZ. Although we cannot locate these events, their moveout suggests that they occur generally west of the line in the area of sparse seismicity that corresponds to deeper levels of the southwesterly dipping Reelfoot thrust fault.

This swarm of events suggests several possibilities. At a minimum, the faults of the NMSZ exhibit a previously unknown level of seismic activity that indicates ongoing physical processes in the fault zone. Without knowing more about the source of these small events, we suggest that they may represent processes similar to ETS or non-volcanic tremor on the San Andreas fault where deep slip on the fault plane seems to be associated with the tremor. Obviously, an observational campaign must be undertaken to locate the source of these kinds of microearthquakes and to determine any time dependence in their occurrence. Since 2005, there has been a controversy surrounding the reality of a strain signal seen across the Reelfoot fault. *Stein (2007)* and others attribute the signal to monument instability or some other GPS processing error while *Smalley et al. (2005)* suggest a resolvable signal showing contraction across the Reelfoot fault. We suggest that times of microseismic swarms will be associated with slow slip events in the deeper levels of the fault system that load higher portions of the fault. A combination of array observations to detect and locate these swarms in conjunction with accurate continuous GPS observations and/or strain observations are needed to test this idea.

Modeling Strong Ground Motion from the 2002 ESEE

The original purpose of this research program was to gather seismic data to place constraints on the velocity and attenuation model for unconsolidated sediments of the Mississippi embayment that could be used to simulate the observed K2 array strong ground motions observed in the ESEE. An initial attempt at this yielded seismic wave forms for the Marked Tree explosion that explained the general features of the 3 component data (Figure 27). The velocity model was derived from acoustic well log data and earthquake P, S, Sp, and Ps phases (Langston 2003). Although the velocity model did well in simulating major arrivals in the data, there remain significant misfits in time, amplitude and frequency that suggest that the model needs refinement.

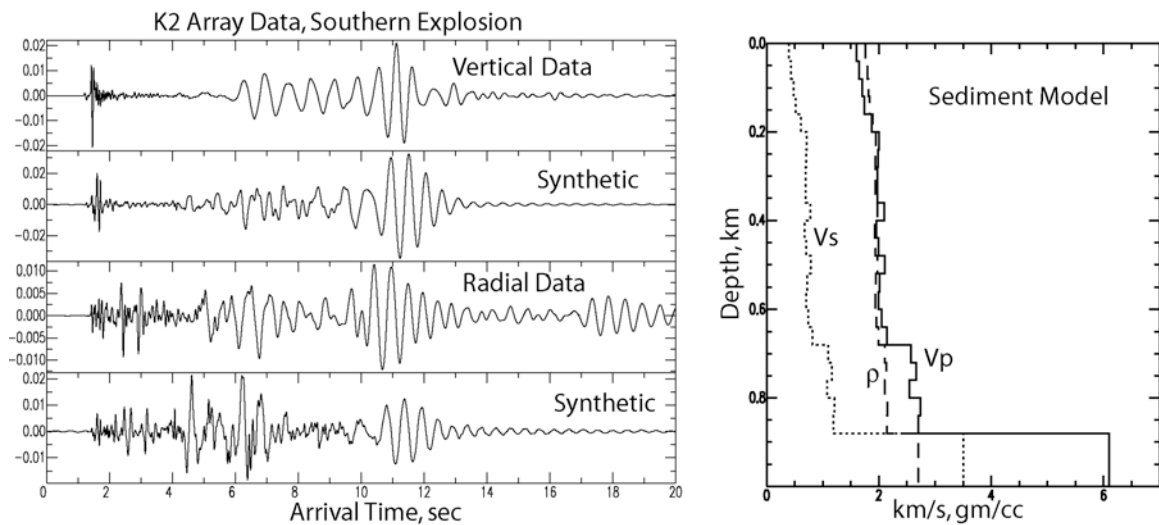


Figure 27 – Observed and synthetic waveforms for the K2 array data recorded for the Marked Tree explosion source. The left panel shows vertical and radial component data with corresponding full wave theory synthetic seismograms using the layered earth model to the right. The general characteristics of the synthetics fit the data in terms of relative amplitudes and arrival times but there are small variations in arrival times suggesting needed changes in the velocity model. In addition, synthetic higher mode Rayleigh waves between 4 and 8 sec arrival times appear to be higher amplitude and higher frequency than the observed.

The purpose of the small scale reflection and refraction experiments was to provide constraints on the velocity structure that could into the wave propagation velocity model. It became apparent as we proceeded with this research that these kinds of constraints, while useful, were not enough to produce a model that could reproduce the waveform data. Refraction/reflection interpretations have their own limitations that cannot cover all of the wave propagation factors needed to model the strong ground motions.

To illustrate this, consider the data from the Mooring shot (Figure 28). The waveforms are relatively simple and there are only a few seismic phases on the vertical and radial components. It would seem that these relatively simple waveforms would also be relatively easy to model. However, it turned out to be difficult.

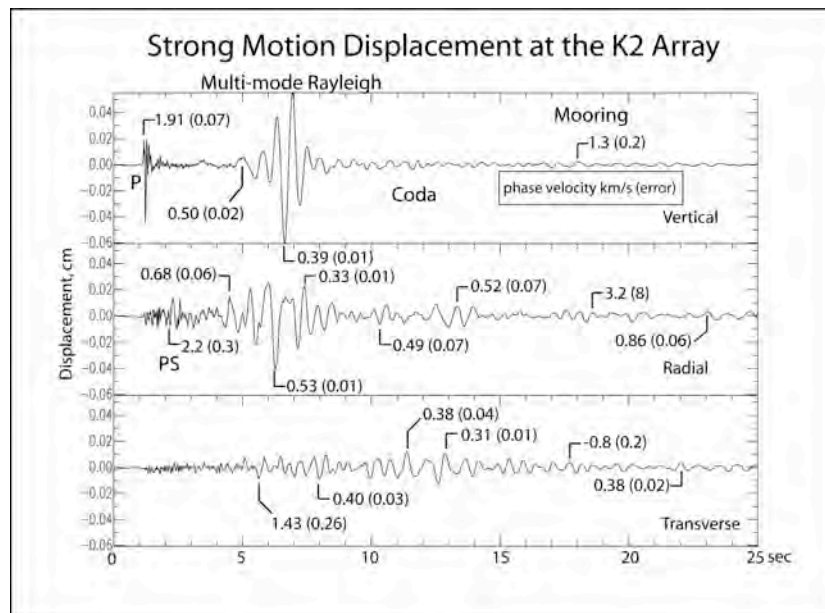


Figure 28 – Data from the Mooring K2 array. Major phases are annotated and phase velocity measurements for individual peaks or troughs shown by the numbers (in km/s) with error (in parantheses).

First arrival travel times from the P and S wave refraction survey at Mooring were fit with low order polynomials and then used to infer a velocity function using the

Herglotz-Weichert technique. Figures 29 and 30 show the arrival time fits and Figure 31 shows the resulting P and S velocity models.

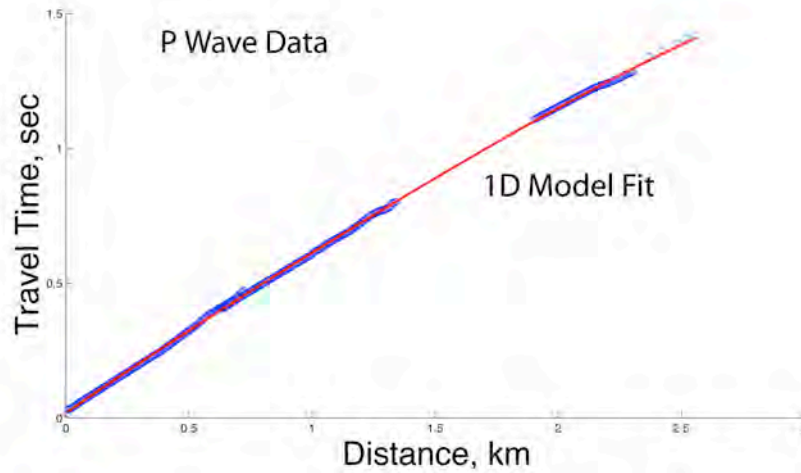


Figure 29 – P wave arrival times (circles) and low order polynomial fit (line).

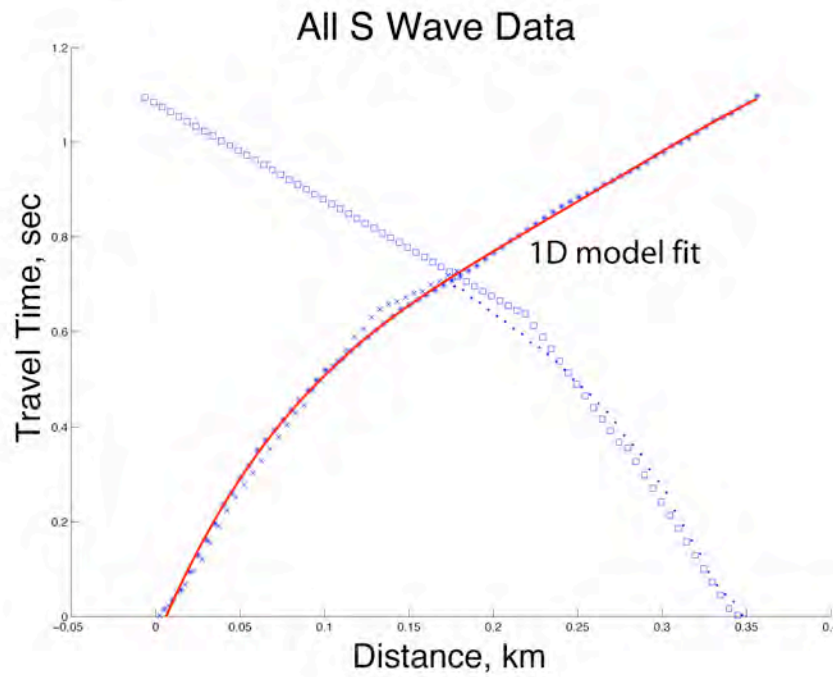


Figure 30 – S wave arrival times (circles and dots) and low order polynomial fit.

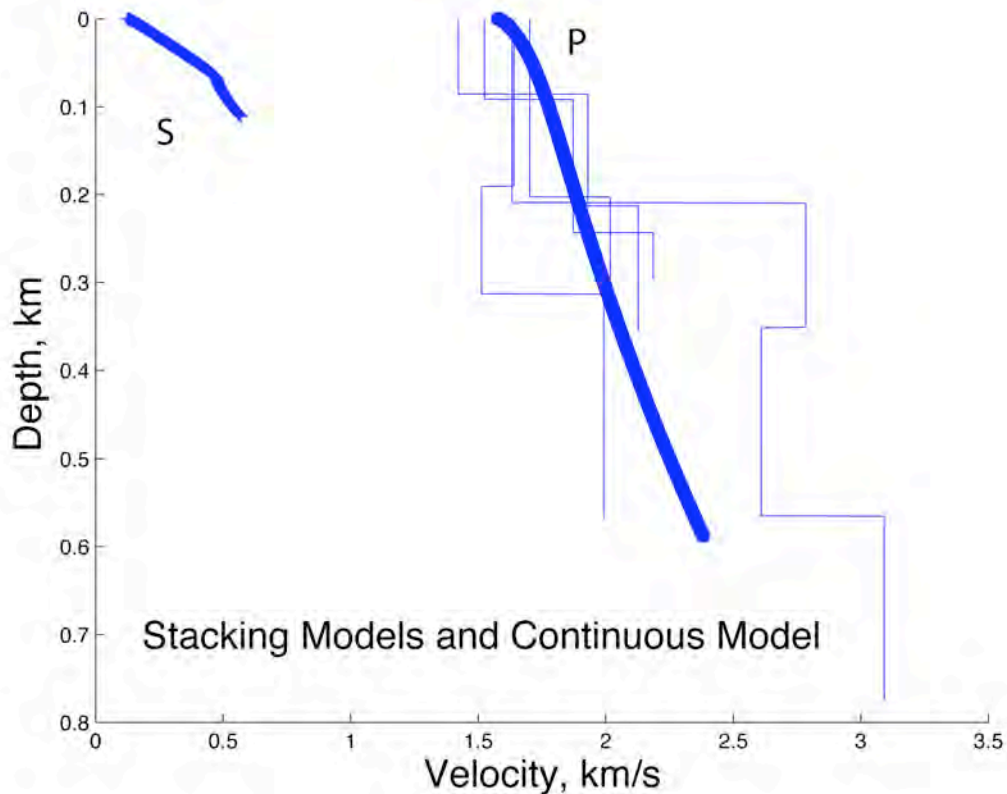


Figure 31 – Continuous P and S wave continuous velocity functions derived from the travel times using the Herglotz-Weichert method. The P wave curve is also superimposed on stacking velocities obtained in the reflection processing.

Figure 31 shows that the S wave refraction experiment did not have the necessary offsets to resolve structure deeper than 100 m. The P wave refraction data did have larger offsets, yet it too probably did not see the basement refraction. These smooth velocity function do provide very important constraints on the velocity structure of the near surface, however, which is very important for the surface wave propagation.

We constructed layered velocity models using these continuous models to use in the full wave theory synthetic seismogram calculations (Figure 32 and 33). Synthetic seismograms are shown in Figure 34 and 35.

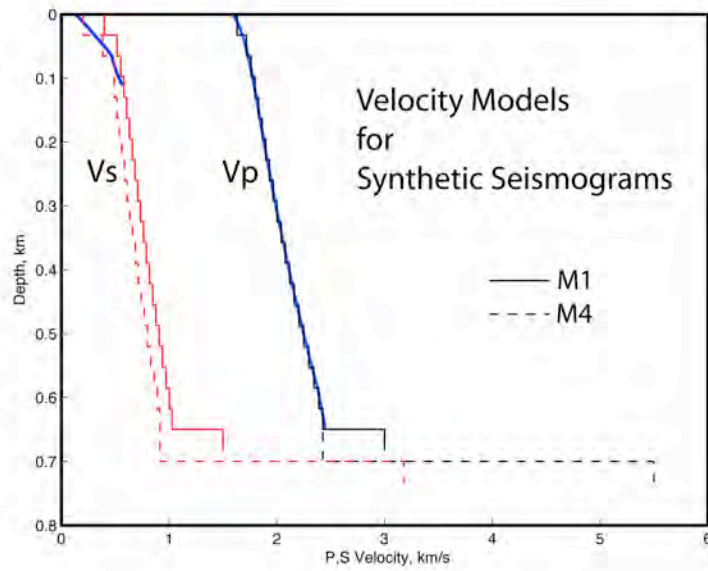


Figure 32 – Velocity models used in the full wave theory synthetic seismogram calculation. Two models are shown that differ in average shear wave velocity and details at the base of the unconsolidated sediments at 700m depth.

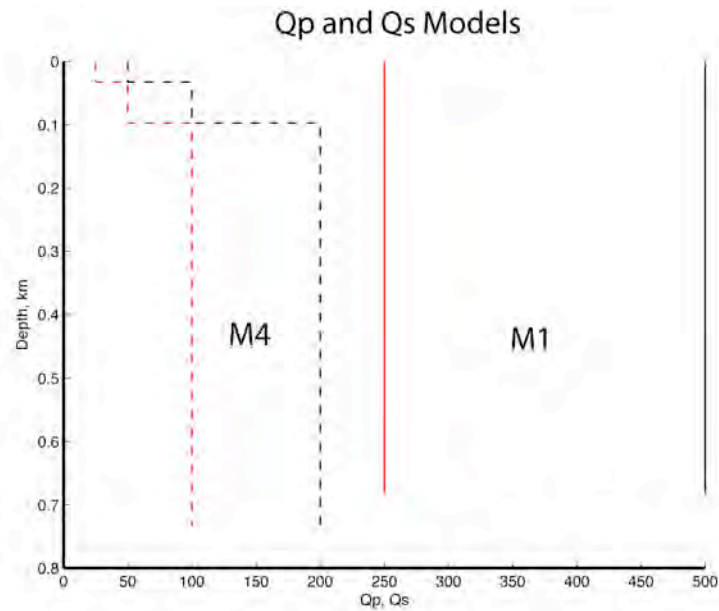


Figure 33 – Qp and Qs models assumed in the synthetic seismogram calculations.

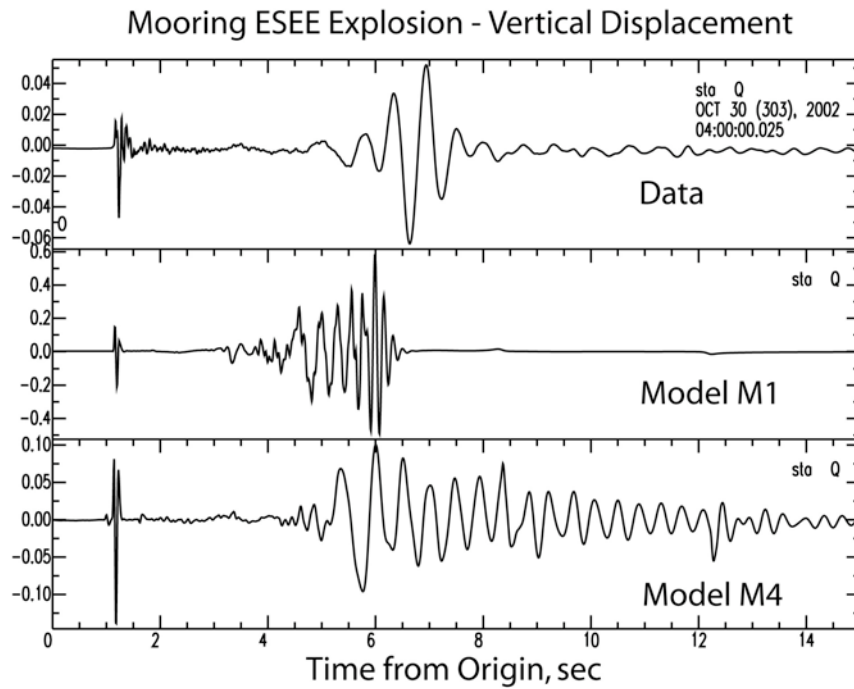


Figure 34 – Vertical component data and synthetic seismograms.

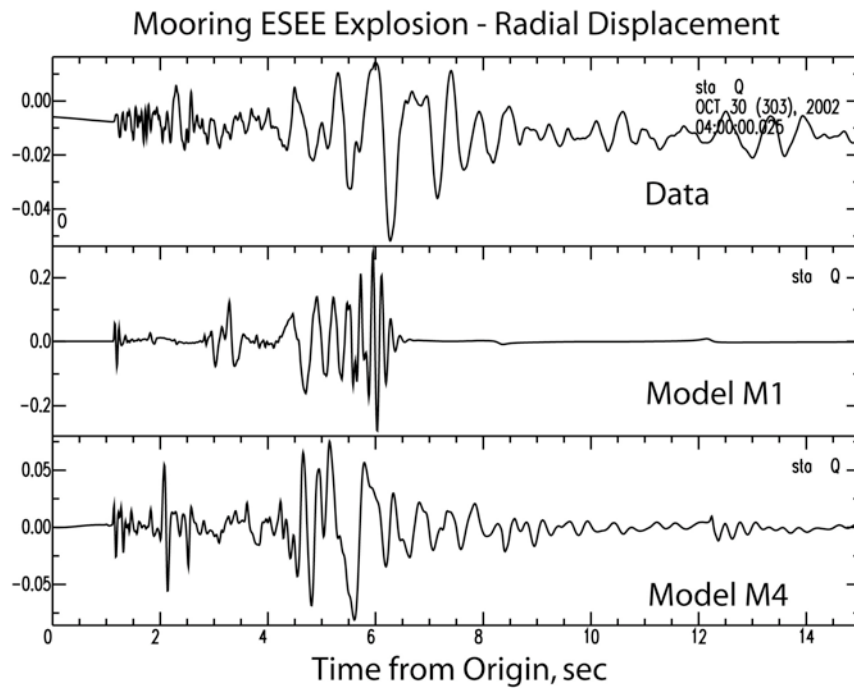


Figure 35 – Radial component data and synthetic seismograms.

Figure 35 shows that very small differences in velocity models have a profound affect on later arriving surface waves. Attenuation structure also has an important effect on the character of the surface waves and the duration of fundamental mode arrivals. For example, the synthetic vertical Rayleigh wave has a long coda due to the very low velocities implied by the refraction model near the surface. If these velocities are part of the model, then attenuation within the upper 10 m or so must be even lower than shown here to remove these coda waves. Again, there are many similar arrivals between the data and synthetics of model M4 but details of arrival time, phase duration, or phase frequency content show room for improvement.

Thus, we have two velocity and attenuation models that approximate characteristics of the observed strong ground motions from the 2002 explosions. The refraction and reflection data put constraints on some aspects of the models, but gross aspects of the waveforms are controlled by attenuation structure and, presumably, by other velocity details within the structure. This continues to be an on-going waveform modeling study and shows how difficult it is to fully understand real wave propagation effects in an area of high earthquake hazards.

DISPOSITION OF DATA SETS

The terms of this grant requires that all data be made freely available to other investigators. We have collected a large suite of broad band array data, network data, reflection/refraction data, and strong ground motion data over a series of field experiments. The P.I.s have given the ESEE data to an outside investigator (A. Jemberie) through a simple tar file of existing Unix directories. We will be constructing an

Antelope data base this summer with the raw waveform data from these experiments and will contribute a SEED volume to the IRIS data center to be publicly available to the community.

BIBLIOGRAPHY OF PUBLICATIONS RESULTING FROM THE WORK

Rieger, D., C.A. Langston, R.A. Williams, D.M. Worley, Velocity structure near the site of the 2002 Embayment Seismic Excitation Experiment explosion from reflection, refraction, and strong motion measurements, , *Eos Trans. AGU*, 88(52), *Fall Meet. Suppl.*, Abstract S11A-0277 (2007).

Langston, C.A., R.A. Williams, M. Magnani, and D.M. Rieger, Possible non-volcanic tremor discovered in the Reelfoot fault zone, northern Tennessee, , *Eos Trans. AGU*, 88(52), *Fall Meet. Suppl.*, Abstract S51D-0764 (2007).

In addition, we are preparing publications on the Blytheville experiment, the H/V array study, the non-volcanic tremor discovery, and structure modeling studies with expected submittal to journals before the end of summer 2008.

REFERENCES

Bodin, P., and S. Horton (1999), Broadband microtremor observation of basin resonance in the Mississippi embayment, central U.S.: Implications for seismic hazard assessment, *Geophys. Res. Lett.*, 26, 903-906.

Bodin, P., et al. (2001), Microtremor observations of deep sediment resonance in metropolitan Memphis, Tennessee, *Engin. Geol.*, 62, 159-168.

- Bromirski, P. D., et al. (1999), ocean wave height determined from inland seismometer data: implications for investigating wave climate changes in the NE Pacific, *J. Geophys. Res.*, *104*, 20,753-720,766.
- Brudzinski, M. R., and R. M. Allen (2007), Segmentation in episodic tremor and slip all along Cascadia, *Geology*, *35*(10).
- Chen, K., et al. (1996), Shear-wave velocity of the sedimentary basin in the upper Mississippi embayment using S-to-P converted waves, *Bull. Seism. Soc. Am.*, *86*, 848-856.
- Dragert, H., et al. (2001), A silent slip event on the deeper Cascadia subduction interface, *Science*, *292*, 1525-1528.
- Haubrich, R. A., et al. (1963), Comparative spectra of microseisms and swell, *Bull. Seism. Soc. Am.*, *53*, 27-37.
- Konno, K., and T. Ohmachi (1998), Ground-motion characteristics estimated from spectral ratio between horizontal and vertical components of microtremor, *Bull. Seism. Soc. Am.*, *88*, 228-241.
- Lachet, C., and P.-Y. Bard (1994), Numerical and theoretical investigations on the possibilities and limitations of Nakamura's technique, *J. Phys. Earth*, *42*, 377-397.
- Langston, C. A. (2003), Local Earthquake Wave Propagation Through Mississippi Embayment Sediments: I. Body Wave Phases and Local Site Responses, *Bull. Seism. Soc. Am.*, *93*, 2664-2684.
- Langston, C. A., et al. (2006), Explosion source strong ground motions in the Mississippi embayment, *Bull. Seism. Soc. Am.*, *96*, 1038-1054.

- Langston, C. A. (2007a), Wave Gradiometry in the time domain, *Bull. Seism. Soc. Am.*, 97, 926-933.
- Langston, C. A. (2007b), Spatial gradient analysis for linear seismic arrays, *Bull. Seism. Soc. Am.*, 97, 265-280.
- Langston, C. A. (2007c), Wave Gradiometry in two dimensions, *Bull. Seism. Soc. Am.*, 97, 401-416.
- Lermo, J., and F. J. Chavez-Garcia (1994), Are microtremors useful in site response evaluation?, *Bull. Seism. Soc. Am.*, 84, 1350-1364.
- Longuet-Higgins, M. S. (1950), A theory of the origin of microseisms, *Philos. Trans. R. Soc. London. Ser. A*, 243, 1-35.
- Miao, Q., and C. A. Langston (2007), Empirical distance attenuation and the local magnitude scale for the central U.S., *Bull. Seism. Soc. Am.*, preprint.
- Nadeau, R. M., and D. Dolenc (2005), Nonvolcanic tremors deep beneath the San Andreas Fault, *Science*, 307, 389.
- Nakamura, Y. (1989), A method for dynamic characteristic estimation of subsurface using microtremor on the ground surface, *QR Railway Tech. Res. Inst.*, 30.
- Rogers, G., and H. Dragert (2003), Episodic tremor and slip on the Cascadia subduction zone: the chatter of silent slip, *Science*, 300, 1942-1943.
- Schwartz, S. Y., and J. M. Rokosky (2007), Slow slip events and seismic tremor at circum-pacific subduction zones, *Rev. of Geophys.*, 45, RG3004.
- Smalley, R., et al. (2005), Space geodetic evidence for rapid strain rates in the NMSZ of central USA, *Nature*, 435(doi:10.1038/nature03642), 1088-1090.

Stein, S. (2007), New Madrid GPS: Much Ado About Nothing? Forum, *EOS Trans. AGU*, 80, 59.